DOCTORAL DISSERTATION SERIES

TITLE An Investigation of the Angular Distribution of Neutrons from the Photo-Disintegration of the Deuteron

AUTHOR Frank Genevese

UNIVERSITY of Michigan DATE 1949

DEGREE Ph.D. PUBLICATION NO. 1213

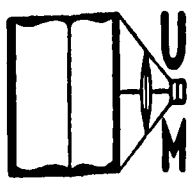

UNIVERSITY MICROFILMS
ANN ARBOR · MICHIGAN

AN INVESTIGATION OF THE ANGULAR DISTRIBUTION OF NEUTRONS FROM THE PHOTO-DISINTEGRATION OF THE DEUTERON

Frank Genevese

A Dissertation Submitted in Partial Fulfillment
of the Requirements for the Degree of
Doctor of Philosophy in the
University of Michigan.

March, 1949.

Committee in Charge:
Professor H. R. Crane, Chairman
Professor E. F. Barker
Professor D. M. Dennison
Assistant Professor R. C. Bartels
Assistant Professor M. L. Wiedenbeck

ACKNOWLEDGMENTS

The author wishes to express his sincere appreciation for the advice and encouragement given him by Professor H. R. Crane under whose direction this research was undertaken. Grateful acknowledgment is also extended to Professor M. L. Wiedenbeck who rendered much valuable criticism throughout the course of the investigation.

The frequent advice contributed by Dr. E. S. Lennox on the theoretical aspects of this problem proved of invaluable aid.

The author wishes to express his indebtedness to the cyclotron staff, Messrs. A. Williams, R. Niehaus, G. Crossman, and R. Wimmer, for their enthusiastic and untiring efforts in assisting in the preparation of the radio-sodium sources and aiding in the conduct of the night operations.

Finally, it is a pleasure to record my appreciation for the stimulation and encouragement afforded me in this investigation through the Horace H. Rackham Special Fellowship appointments for the school years 1947-1948 and 1948-1949.

TABLE OF CONTENTS

CONTENTS (cont'd)

CONTENTS (cont'd)

ILLUSTRATIONS

LIST OF TABLES

CHAPTER I

INTRODUCTION

A. Statement of the Problem

A nuclear analogue of the atomic photoelectric effect was first observed by Chadwick and Goldhaber (1934). By irradiation with sufficiently hard gamma rays, the deuteron was found to disintegrate into a proton and a neutron. The manner in which the deuteron in its ground state is dissociated by this process may lead to valuable information on the properties of two-nucleon systems. Thus, the gamma ray threshold frequency for photo-disintegration yields immediately the binding energy of the deuteron. In addition, the angular distribution with which the neutrons (or protons) are ejected gives rise to important theoretical inferences. Properly assessed, such information derived from the simplest of all nuclear systems could serve as an invaluable source of experimental evidence regarding the nature of the forces holding the neutron and proton together. It is this character of the specific forces acting between nucleons which constitutes the central problem of present-day nuclear physics.

Within the past decade, a considerable amount of effort has been expended by numerous investigators toward the experimental determination of the deuteron binding energy. At the

present time, this important physical constant is presumably known to within an accuracy of 2%. Comparable success, however, has not attended the experimental efforts of the investigators who have attempted the measurement of the angular distribution of the photo-ejected nucleons. Unfortunately, owing to the low intensity effects involved, such measurements are very difficult, and it has not been possible to attain the accuracy required for verification of the theoretical analysis from the empirical data.

In the photo-disintegration of the deuteron, it is necessary to take into consideration not only the influence of the electric field of the gamma ray (the photoelectric effect), but also that of the magnetic field (the photomagnetic effect). In the former, the disintegrations are the result of electric dipole transitions of the deuteron (electric quadrupole transitions play only a negligible role); in the latter, a magnetic dipole transition is involved. It has been shown that the above two effects result in a superposition of a ^3P, i.e. $\sin^2$, distribution and a spherically symmetrical ^1S distribution, respectively, for the ejected nucleons in the barycentric system. For photons whose energy is not too high, and therefore of small momentum, the barycentric system of reference may be identified with the laboratory system.

Since the photo-disintegration differential cross section consists of two terms of different origin, it is possible to distinguish one from the other by the difference in their depen-

dence on the angle of ejection of the nucleons with respect to the direction of the incident photon. Thus, experimental evaluation of the ratio of intensities of the ejected neutrons at two different directions to that of the incident radiation is required. This leads to an evaluation of the ratio of the total magnetic and electric cross sections, $\tau = \frac{\sigma_m}{\sigma_{el}}$, which may then be compared with that calculated from theory.

This dissertation reports the method, results, and conclusions of an attempt to determine experimentally a more precise value for the ratio of the total photomagnetic to the total photoelectric cross section of the deuteron at a gamma ray energy of 2.76 Mev. In several important respects the experimental methods employed represent improvements over former techniques. A geometrical configuration for the components of the apparatus has been selected which is designed to enhance the recorded neutron intensity while simultaneously reducing the angular opening allowed the primary gamma rays and photo-neutron beam. This has led to an increase in neutron intensity by a factor of 10, and a reduction of over 30% in the angular opening over experimentation previously reported. The recorded intensity has also been improved by the use of relatively strong gamma ray sources and by the construction of a neutron counter whose efficiency is increased by a factor of 5 through the use of BF_3 gas enriched in B^{10}. Finally, the experimental corrections for the scattering of the neutrons by the heavy water and by the walls of the room have been

essentially eliminated by the choice of geometry and by the suspension of the apparatus outdoors at least 90 feet away from all objects.

B. Résumé of Results

Guided by theoretical analysis, we assume an angular distribution for the photo-neutrons of the form $a + b \sin^2\gamma$, where γ represents the angle between the photo-neutrons and the direction of the incident gamma rays. From the experimental results obtained, we are led to a final weighted mean for the quotient, $\frac{a}{b}$, having the value

$$\frac{a}{b} = 0.196 \pm 0.024$$

In terms of the ratio of the photomagnetic to the photoelectric cross section, we obtain

$$\tau = 0.295 \pm 0.036$$

for gamma rays of 2.76 Mev energy. This leads to the following value for the ratio of the photomagnetic cross section to the total photo cross section.

$$\frac{\tau}{\tau + 1} = 0.228 \pm 0.028$$

We are led by the overall results of this investigation to conclude that, within the accuracy of the experimental error, the observed total angular distribution of the photo-neutrons

arising from the photo-disintegration of the deuteron conforms with the theoretical prediction that the distribution is anisotropic with the ejected particles emerging predominantly at right angles to the direction of the incident gamma radiation. The prediction, on theoretical grounds, that this total angular distribution may be resolved into an isotropic component arising from magnetic interaction of the photon with the deuteron and an anisotropic component arising from electric interaction with the deuteron is consistent with the results of this investigation. That the relative magnitude of these two components conforms to the theoretical value as predicted by equation (14) is in general verified. However, neither the accuracy of the present experimental results, nor the ambiguities relating to the values of the physical constants (Table XV) appearing in equation (14) permit unequivocal conclusion that a precise agreement exists between experiment and theory. We may say categorically, however, that within the generality of "order of magnitude" an agreement is found to exist at the gamma ray energy of 2.76 Mev.

In contrast with early photo-disintegration experiments, the existence of a magnetic component is verified beyond any doubt. At the photon energy involved, the total cross section for the magnetic component appears to be approximately 30% of that for the electric component. Further, it has been shown that σ_m constitutes approximately 23% of the total photo-disintegration cross section.

In consequence of the difficulties attending the measurement of the weak effects associated with photo-disintegration by current techniques, verification of the existence of the additional $^3D - {}^3P$ and $^3D - {}^1D$ transitions (see Table I) predicted by non-central force theory, lies well beyond present experimental capabilities. It is highly improbable that a more sensitive technique following the present experimental scheme can be devised to resolve these lower intensity effects. This limitation, plus the difficulties encountered in making more precise measurements on the predominant $^3S - {}^3P$ and $^3S - {}^1S$ transition products, seriously restrict the inferences one may draw on the basis of experimental results. Thus, supporting evidence regarding such fundamental nuclear properties as the character of the nuclear forces or, for that matter, the range of these forces must rely upon information not currently available from experiments on photo-disintegration.

CHAPTER II

THEORY OF NUCLEAR PHOTOEFFECT

A. Photo-disintegration of the Deuteron

1. General:

In 1934 Chadwick and Goldhaber[1,2] succeeded in producing the photo-disintegration of the deuteron into a neutron and a proton by use of the gamma rays from ThC' of 2.62 Mev energy. The reaction has the form

$$H^2 + h\nu = H^1 + n^1 + E \qquad (1)$$

where $h\nu$ is the gamma ray energy and E is the total kinetic energy of neutron and proton produced in the process. Since the gamma ray momentum is negligible, the proton and neutron, considered as having equal masses, have opposite momenta and share the energy, E, equally. The absorption of the gamma ray by the deuteron gives rise to a process quite analogous to the photoelectric effect in atoms. The gamma ray produces a transition of the deuteron from the ground state to a state of positive energy, E, such that

$$E = h\nu - W_1 \qquad (2)$$

Here W_1 represents the binding energy of the deuteron.

In the initial investigation, the above workers were able to determine the number of ions produced by a proton formed in the photo-disintegration process and from this to assign a value to the binding energy. With the number of ions so produced being set at about 7200, and with an energy requirement of 33 ev for each ion produced, the kinetic energy of the proton is therefore 33 x 7200 = .24 Mev. From this we obtain for the approximate value of the binding energy of the deuteron the value $W_1 = 2.62 - 2(.24) = 2.14$ Mev.

More accurate measurements of the deuteron binding energy have been performed by Stetter and Jentschke[3], Wiedenbeck and Marhoefer[4], Myers and VanAtta[5], and Kimura[6]. An exhaustive survey and analysis of the literature have been made by Stevens[7]. He adopts as the best value 2.187 $\pm$ 0.011 Mev. Since publication of this value, Bell and Elliott[8] have re-investigated the gamma ray accompanying the capture of a neutron by a proton in a magnetic lens beta-ray spectrometer. They report the surprisingly different value of 2.237 $\pm$ 0.005 Mev for the binding energy of the deuteron.

Our present interest lies in the differential cross section for the photo-disintegration process. The cross section for gamma ray absorption is given by the formula

$$\sigma = \frac{8\pi^3\nu}{c} \left| M_{OE} \right|^2 \qquad (3)$$

where ν is the frequency of the incident photon, and M is the matrix element of the electric or magnetic dipole moment

for the transition from the ground state to the state of energy E. Photo-disintegration is seen to take place by two different processes.

We consider the radiation as an incoming plane wave. The interaction energy between proton and electric field, $\bar{\mathcal{E}}$, will be $-e\bar{\mathcal{E}}\cdot\bar{r}$, where $\bar{r}$ is the proton coordinate vector relative to the neutron; the interaction energy between the magnetic moment of both the proton and neutron with the magnetic field $\bar{H}$ will be $-(\bar{\mu}_p + \bar{\mu}_n)\cdot\bar{H}$. Here $\bar{\mu}_p$ and $\bar{\mu}_n$ denote the magnetic moment of proton and neutron, respectively.

2. Electric Interaction

We shall first discuss the results of theory as applied to the electric interaction which has been developed by Bethe and Peierls[9] and others[10, 11, 12, 13]. The photoelectric effect is the result of a transition of the deuteron from the ^3S ground state to a final state which must be a p-state in order to produce a non-vanishing matrix element. Since no stable p-state exists, the transition must be one to a p-state of the continuous spectrum which has zero angular momentum around the direction of polarization of the incident gamma ray. Hence, the electric photoeffect involves a $^3S - {}^3P$ transition by electric dipole interaction.

The evaluation of the photoelectric cross section rests upon the assumption that the force between neutron and proton does not influence the final p-state - an assumption which is

valid provided the range of the force, a, is small compared to the wave length $\lambda = \hbar/(ME)^{\frac{1}{2}}$ corresponding to the state E. Therefore, the p-state wave function will have the same form as if the neutron and proton were free. Bethe and Bacher[14] have evaluated the matrix element of the electric dipole moment and thence its contribution to the photoelectric cross section under the above assumption. Since only the proton has a charge, e, and since its coordinate relative to the center of gravity of the deuteron is $\frac{1}{2}\bar{r}$, we have

$$M_{0E}^{el} = \tfrac{1}{2}e\int \psi_i z\, \psi_f d\tau \qquad (4)$$

where z is in the direction of polarization of the gamma ray. ψ_i is the wave function of the deuteron in the ground state and ψ_f is the wave function for free particles in the final state normalized per unit energy. It is found that the probability of ejection of a photo-proton or photo-neutron into unit solid angle at an angle θ to the direction of polarization of the incident gamma radiation is proportional to $\cos^2\theta$. On averaging over all directions of polarization, since the radiation is unpolarized in general, one finds that the number of photo-neutrons projected into solid angle, $d\Omega$, will be proportional to $\sin^2\gamma$ where γ is the angle between the direction of the incident gamma ray and the ejected neutron as:

$$d\sigma_{el}(\gamma) = \frac{\hbar e^2}{Mc}\,\frac{W_1^{\frac{1}{2}}\,E^{3/2}}{(E+W_1)^3}(1+\alpha a)\sin^2\gamma\, d\Omega \qquad (5)$$

Here, M is the neutron mass, a is the width of the rectangular potential well, and $\alpha = \sqrt{MW_1}/\hbar$. The factor $(1 + \alpha a)$ enters from the normalization of the wave function in the ground state, $^3S_1$.

The angular distribution of the photo-neutrons (or photo-protons) due to the photoelectric effect is thus a $\sin^2$ distribution with the ejected particles emerging mostly at right angles to the direction of the incident gamma radiation.

The total cross section for the electric photoeffect found by averaging over all directions of the proton or neutron is, after the results of Bethe and Bacher,

$$\sigma_{el} = \frac{8\pi}{3} \frac{e^2}{\hbar c} \frac{\hbar^2}{M} \frac{W_1^{\frac{1}{2}} E^{3/2}}{(E + W_1)^3} (1 + \alpha a) \qquad (6)$$

This photoelectric cross section vanishes at the threshold, $E = 0$, and increases as $E^{3/2}$ with increasing gamma ray energy until a maximum of $26.6 \times 10^{-28} cm^2$ is reached at $h\nu = 2W_1$. At still higher energies the cross section again decreases as $E^{-3/2}$.

3. Magnetic Interaction

The photomagnetic disintegration of the deuteron has been shown by Fermi[15] to be the inverse process of the magnetic capture of thermal neutrons by protons which can be understood qualitatively as a magnetic dipole transition from a ^1S level[16] to the bound ^3S level of the deuteron.

In the nuclear photomagnetic effect, the initial state is the $^3S_1$ ground state. The final state must be an s-state otherwise the integration over angles for the matrix element, M, in equation (3) will vanish. Further, because of the dependency of the neutron-proton force upon spin, the wave functions in the initial and final state are not orthogonal. Thus the matrix element does not vanish and a ^3S - ^1S transition due to the magnetic dipole moment is allowed. This transition is forbidden for the electric dipole. To calculate the transition probability using the magnetic dipole moment, it is necessary to evaluate the matrix element

$$M_{OE}^{mag} = \frac{e\hbar}{2Mc} (\mu_p - \mu_n) \int \psi_i \, \psi_f \, d\tau \qquad (7)$$

where ψ_i is the wave function which is approximately the same as that used earlier, and ψ_f is the wave function for the ^1S state corresponding to energy E, angular momentum $l = 0$, opposite spin of proton and neutron, and normalized to unit energy.

The contribution of the magnetic photoeffect, especially important near threshold energies, will be isotropic in angle in contrast to the results for electric photoeffect. The effect of the gamma radiation is to alter the spins from a parallel to an anti-parallel position; therefore, the neutron and proton fly apart with equal probability in all directions. On evaluating the matrix elements of the magnetic dipole moment using equations (3) and (7), Bethe and Bacher[14] have

obtained the following expression for the photomagnetic cross section with nuclear forces taken into account in both initial and final s-states.

$$\sigma_m = \frac{2\pi}{3} \frac{e^2}{\hbar c} \frac{\hbar^2}{M^2c^2} \frac{W_1^{\frac{1}{2}} E^{\frac{1}{2}} (W_1^{\frac{1}{2}} \pm |W_o|^{\frac{1}{2}})^2}{(E \pm W_1)(E \pm |W_o|)} (\mu_p - \mu_n)^2 \qquad (8)$$

where μ_p and μ_n are the magnetic moments of proton and neutron, respectively, in units of the nuclear magneton $e\hbar/2Mc$, and W_o is the binding energy of the ^1S level, the plus or minus sign holding according to whether the singlet state of the deuteron is virtual or real.

Except very near threshold σ_m is smaller than σ_{el}. At high energies both magnetic and electric cross sections decrease as $E^{-3/2}$. At low energies the electric cross section behaves as $E^{3/2}$, whereas the magnetic cross section behaves as $E^{\frac{1}{2}}/(E \pm W_o)$. The cross-over point is at an energy of approximately 2.42 Mev.

Since the final states for the two processes are different, there is no interference effect entering and the total photo cross section is given simply by

$$\sigma = \sigma_m + \sigma_{el} \qquad (9)$$

4. Energy of the Singlet State

To make use of equation (8) we must know the energy of the ^1S level. Wigner[16] showed from theoretical considerations that the large cross section for the scattering of slow neutrons by

protons leads to the prediction that this energy has a value of about 100,000 ev. From an experimental determination of the scattering cross section of protons for slow neutrons, Hanstein[17] has shown that the nucleus of the deuteron has a ^1S level with an energy W_o equal to 66,000 ev. However, the scattering cross section does not depend on whether this level is real or virtual. For this reason, it is necessary to resort to other means to determine which sign in equation (8) applies. We shall consider in the following section the various lines of evidence which indicate that the ^1S level is virtual.

5. Sign of the Singlet State

We shall now consider four separate experimental methods which in principle should serve to settle the question of the sign of the singlet state of the deuteron.

a. Neutron Capture by Protons

As mentioned earlier, the photomagnetic disintegration of the deuteron was predicted by Fermi to be an inverse process to that of slow neutron capture by protons. The action here involves the capture of a neutron by a proton with the emission of a gamma ray which carries off the excess energy. By a statistical argument[14,18] it can be shown that the ratio of the capture cross section to the photomagnetic cross section is proportional to the square of the ratio of the momenta of the emitted photon and of the emitted neutron in the disintegration, as:

$$\frac{\sigma_{cap}}{\sigma_m} = \frac{3}{2}\left(\frac{p_\gamma}{p_n}\right)^2 \qquad (10)$$

Using equation (8) for σ_m, we get from equation (10) that

$$\sigma_{cap} = \pi \frac{e^2}{Mc^2}\frac{\hbar}{Mc}\left(\frac{2W_1}{E_o}\right)^{\frac{1}{2}} \frac{(W_1^{\frac{1}{2}} \pm W_o^{\frac{1}{2}})^2 (W_1 \pm \frac{1}{2}E_o)}{(W_o \pm \frac{1}{2}E_o) Mc^2}(\mu_p - \mu_n)^2 \qquad (11)$$

where E_o is the energy of the incident neutrons in the laboratory system. Again, the plus or minus sign stands according to whether the singlet state of the deuteron is virtual or stable. The value of σ_{cap} is proportional to $E_o^{-\frac{1}{2}}$ and is largest for slow neutrons. For thermal neutrons, $E_o \sim .025$ ev and $\sigma_{cap} \sim 0.3$ barns.

It is of interest to note that by employing equation (11) into (8) so as to express the photomagnetic cross section in terms of the capture cross section of the proton for neutrons of energy E_o, we get the simple relation:

$$\sigma_m = \frac{\sqrt{2}}{3} E_o^{\frac{1}{2}} E^{\frac{1}{2}} Mc^2 \frac{(W_o \pm \frac{1}{2}E_o)}{(E \pm W_1)(E \pm W_o)(W_1 \pm \frac{1}{2}E_o)} \cdot \sigma_{cap} \qquad (12)$$

Hence, in principle it is not necessary to know the magnetic moments of proton and neutron. σ_m can be obtained for all gamma ray energies once the energy of the ^1S level, W_o, is established provided σ_{cap} is known for neutrons of one energy, E_o. Equation (12) gives satisfactory agreement with (8) on using the capture cross section for thermal neutrons, $\sigma_{cap} = 3.1 \times 10^{-25} cm^2$, as reported by Schultz and Goldhaber[19].

Of further interest is the fact that equation (12) does not contain explicitly the sign of the ^1S level.

To return now to the question of experimentally varifying this sign, we consider the mean lifetime, $\bar{t}$, of a neutron in hydrogenous material. This is related to the capture cross section for neutrons by protons. The number of captures per second is, by definition,

$$\frac{1}{\bar{t}} = N \sigma_{cap} \bar{v} \qquad (13)$$

where $\bar{v}$ is the velocity of the neutrons and N is the number of hydrogen atoms per cubic centimeter. For thermal neutrons we take $\bar{v} = 2.2 \times 10^5$ cm/sec and for water we take $N = 6.73 \times 10^{22}$ atoms/cc.

By using the expression for σ_{cap} from equation (11) into (13) we have for the 2.62 Mev gamma rays of ThC' that

$\bar{t} = 2.9 \times 10^{-4}$ sec (if singlet virtual state exists)

$\bar{t} = 6.3 \times 10^{-4}$ sec (if singlet real state exists)

In 1937, Frisch, Halban, and Koch[20] obtained an experimental value for the mean life of neutrons in water and found $\bar{t} = 2.7 \times 10^{-4}$ seconds. More recently a redetermination by Manley, Haworth, and Luebke[21] yields the value $\bar{t} = 2.05 \times 10^{-4}$ sec. From this latter result the average capture cross section, σ_{cap}, for thermal neutrons is found to be 3.3×10^{-25} cm^2. This value compares favorably with the value of 3.1×10^{-25} as reported by Schultz and Goldhaber[19] in 1945.

b. Ortho- and Para-Hydrogen Scattering

In 1936 Teller first pointed out that a comparison of the scattering of neutrons by ortho- and para-hydrogen would provide an experimental test of the spin dependence of the neutron-proton interaction. In addition, however, such a comparison also provides information on the spin of the neutron and on whether the singlet state of the deuteron is real or virtual. (Reference 18, page 49)

When all necessary corrections are applied, the scattering cross sections to be compared with experimental results have the form (see Bethe's text, pg. 53, or reference 22)

$$\sigma_{para} = 6.47\ (3a_1 \neq a_o)^2$$

$$\sigma_{ortho} = 6.29\left\{(3a_1 \neq a_o)^2 \neq 2(a_o - a_1)^2\right\} \neq 1.45\ (a_o - a_1)^2$$

where a_o is the amplitude of the scattered neutron wave in the singlet state (para-hydrogen) and a_1 is the corresponding triplet amplitude (ortho-hydrogen). At low energies the scattered amplitudes for the triplet and singlet states will have opposite signs if the singlet state is virtual and the ratio of the ortho to the para cross section will be about 35. For the same sign, this ratio will be about 1.4. Hence, experimental evaluation of the ortho and para cross sections is sufficient to determine a_o and a_1. The results of DeWire, Sutton and others at the Los Alamos Laboratory[23] represent perhaps the most accurate evaluation of these cross sections:

$$\sigma_{para} = 3.97 \times 10^{-24} \text{ cm}^2$$
$$\sigma_{ortho} = 124 \times 10^{-24} \text{ cm}^2$$

From this it follows that the singlet scattering amplitude, a_o, is opposite in sign to that of the triplet scattering amplitude, a_1. In addition, assignment of a positive value to a_o will be required to account for the large ratio of ortho to para scattering as observed.

c. Neutron Diffraction

Just as the measurement of the coherent scattering of neutrons by hydrogen permits the evaluation of the scattering amplitudes characteristic of the two spin states, viz., when the neutron and proton spins are parallel or anti-parallel, so also the coherent scattering of neutrons by hydrogen-containing crystals yields similar information[24].

Again using a_1 and a_o to represent the triplet and singlet scattering amplitudes of a free proton when the spins of the proton and incident neutron are, respectively, parallel and anti-parallel, then

$$f_H = 2(\tfrac{3}{4}a_1 + \tfrac{1}{4}a_o)$$

gives the coherent scattering amplitude for hydrogen in a crystal. Also the total scattering cross section of a free proton is

$$\sigma_f = 4\pi(\tfrac{3}{4}a_1^2 + \tfrac{1}{4}a_o^2)$$

Neutron diffraction experiments on hydrogen-containing crystals yield, for the coherent scattering amplitude, the value

$$f_H = 0.472 \times 10^{-12} \text{ cm}$$

The total scattering cross section for a free proton as reported by Hanstein[17] is

$$\sigma_f = 21 \times 10^{-24} \text{ cm}^2$$

Thus one obtains for the triplet scattering amplitude the value

$$a_1 = -0.498 \times 10^{-12} \text{ cm}$$

and for the singlet scattering amplitude the value

$$a_o = +2.44 \times 10^{-12} \text{ cm}$$

Hence neutron diffraction experiments lead to the same overall conclusions as found from neutron scattering experiments on ortho- and para-hydrogen.

d. Ratio of the Photoeffects

The expression (6) for the photoelectric cross section due to electric dipole interaction does not depend upon the sign of the singlet state of the deuteron. However, the photomagnetic cross section (8) due to magnetic dipole interaction does depend upon this sign. For this reason the

relative contributions of the two photoeffects will depend upon whether the ^1S state is real or virtual. The experiments tending to confirm or deny the question of stability of the ^1S state of the deuteron through observations on the relative contribution of the two photoeffects have taken the form of photo-neutron or photo-proton intensity measurements at 0° and 90° to the incident gamma radiation.

However, the great difficulty attending such measurements, because of the rather weak effects produced with even moderately strong gamma ray sources, makes such experiments difficult.

In view of the fact that these experiments are the forerunners of the present investigation, a detailed discussion of these works is deferred to the next chapter in which the earlier experimental results on photo-disintegration are summarized.

By taking the ratio of the photomagnetic to the photoelectric cross section as given in equations (8) and (6), we obtain the ratio of probabilities of magnetic to electric effect. Designating this ratio as τ, we get (Reference 14, pg. 125)

$$\tau = \frac{(\mu_p - \mu_n)^2}{4(1 \mp \alpha a)} \frac{(E \mp W_1)^2}{(E \mp W_0)} \frac{(W_1^{\frac{1}{2}} \pm W_0^{\frac{1}{2}})^2}{EMc^2} \qquad (14)$$

In terms of this ratio, the number of neutrons emitted into the solid angle $\sin\gamma' d\gamma'$ will be proportional to[14]

$$\sigma(\gamma')\sin\gamma' d\gamma' = (\sin^2\gamma' \mp 2/3\tau)\sin\gamma' d\gamma' \qquad (15)$$

where γ is the angle between the direction of propagation of the gamma ray and the path of the ejected neutron. Hence, by experimentally measuring the number of neutrons projected in two different directions relative to the incident gamma rays, it is possible to evaluate the coefficient τ quantitatively. An experimental means is thereby provided for comparison of the relative contributions of the photomagnetic to the photoelectric effect as predicted by theory. This is essentially the method employed in the present investigation wherein the Na^{24} gamma rays of 2.76 Mev are used.

B. Influence of Non-Central Forces

Rabi and co-workers have experimentally shown that the deuteron possesses an electric quadrupole moment. This fact has the consequence that the wave function of the deuteron in the ground state is not spherically symmetric but is dependent upon the angle between the total spin direction and the line joining the neutron and proton. The deuteron thus appears to have a charge distribution which is a spheroid, prolate along the spin axis.

Since purely central forces designated by V(r), where r is the distance between nuclei, give no mixing of states with different orbital angular momenta, the presence of the angular dependence of the wave function makes it necessary to introduce forces which are dependent upon the angle between the line joining the nuclei and the total spin axis. These are the so-called tensor forces.

Rarita and Schwinger have shown that, for 4% of the time, the deuteron is in the d-state for which L = 2. Thus, the ground state of the deuteron becomes the $^3S_1 + {}^3D_1$ state, when non-central forces are taken into account. To the photoelectric cross section involving the $^3S - {}^3P$ transition, we have now to add an isotropic term due to the transition $^3D_1 - {}^3P$. The angular dependence now becomes $\sin^2\gamma + 0.0007$. The isotropic term is so small it will probably never be observed by current techniques. The effect of the tensor forces is to reduce the photoelectric cross section slightly from that predicted by central force theory. This is due to the fact that the presence of the ^3D state decreases the percentage of the ^3S state in the wave function without itself contributing appreciably to the cross section. At 2.62 Mev, the photoelectric cross section predicted by non-central force theory is 11.99×10^{-28} cm^2 as compared to 12.31×10^{-28} cm^2 from central force theory.

With non-central forces, the photomagnetic cross section at 2.62 Mev is reduced from 3.4×10^{-28} cm^2 to 3.28×10^{-28} with the angular distribution now altered by the presence of an anisotropic term: $(1 - 0.0035 \cos^2\gamma)$. This term results from the $^3D - {}^1D$ transition and is well beyond experimental detection.

The total cross section at 2.62 Mev is 15.27×10^{-28} cm^2 with an angular dependence of $(\sin^2\gamma + 0.182)$. This is to be compared with Graham and Halban's experimental results

which give 10 x 10^{-28} cm^2 with an angular dependence of $\sin^2 \gamma$ $\neq$ 0.26 $\leq$ 0.08.

We may conveniently tabulate these results of theory and experiment as applied to the 2.62 Mev gamma rays of ThC'. This is shown in Table I. The experimental values reported here are those given by Graham and Halban[25] and discussed in the next chapter. The experimental magnetic cross section of 2.8 x 10^{-28} cm^2 is a corrected value from that reported by these authors. Through error, the published experimental cross section was given as 3.9 x 10^{-28} cm^2.

TABLE I

COMPARISON OF THEORETICAL AND EXPERIMENTAL PHOTO-DISINTEGRATION CROSS SECTIONS (x 10^{28} cm^2) FOR 2.62 Mev GAMMA RAYS

INTERACTION:		ELECTRIC	MAGNETIC	TOTAL
EXPERIMENTAL	Distribution	$\sin^2\gamma$	Isotropic	$\sin^2\gamma + .26 \pm .08$
	Cross section	7.2	2.8*	10
CENTRAL FORCE THEORY	Distribution	$\sin^2\gamma$	Isotropic	
	Cross section	12.31	3.4	15.71
	Transition	$^3S - {}^3P$	$^3S - {}^1S$	
NON-CENTRAL FORCE THEORY	Distribution	$\sin^2\gamma + .0007$	$1 - .0035\cos^2\gamma$	$\sin^2\gamma + .182$
	Cross section	11.99	3.28	15.27
	Transition	$^3S - {}^3P$ $^3D - {}^3P$	$^3S - {}^1S$ $^3D - {}^1D$	

* corrected value

CHAPTER III

EXPERIMENTAL METHODS

A. Historical Summary

The first experiments on the photo-disintegration of the deuteron at low energies were performed by Chadwick and Goldhaber[1] in 1934 using the 2.62 Mev gamma rays from ThC'. This pioneer work served to establish the possibility of producing nuclear photo-disintegration in which the $_1H^2$ atom splits up under the action of sufficiently hard gamma rays. Because of the fact that observations were made on deuterium gas irradiated in a cloud chamber and also because of the possibility of large error in the measured gamma ray intensity, determination of the cross section in this way was difficult. Later[2], using a linear amplifier for measurement of the protons produced in the reaction, they calculated a value for the cross section of about 6×10^{-28} cm^2.

Again in 1937, Chadwick, Feather and Bretscher[26] obtained 65 photo-proton tracks produced in a cloud chamber by 2.62 Mev gamma rays. These authors found that the angular distribution of the tracks conformed to a $\sin^2$ law. However, no evidence could be found of a uniform distribution as required by the photomagnetic effect despite the fact that at this energy an appreciable contribution should be expected. Undoubtedly this deficiency could readily be attributed to the small

number of tracks available, as the authors point out. The relative contribution of the magnetic effect to the electric effect as we have seen depends upon the sign of the ^1S level. For 2.62 Mev gamma rays, the ratio of the number of protons or neutrons observed in the 0° direction to that in the 90° direction is expected to be (see reference 29, below)

$$I_0/I_{90} = .29 \quad \text{(for a } ^1S \text{ virtual level)}$$

$$I_0/I_{90} = .13 \quad \text{(for a } ^1S \text{ real level)}$$

The Chadwick, Feather, and Bretscher results show the contribution from the magnetic effect to be even lower than that expected for a real level. In consequence of this fact, these authors are tempted to conclude that the ^1S state is stable.

In the same year as the Chadwick, Feather and Bretscher experiment, Richardson and Emo[27,28] made a cloud chamber study on deuterium gas at approximately one atmosphere pressure. Using Na^{24} gamma rays from an activated NaF source of 12 mg radium equivalent, they obtained 42 measurable tracks. The angular distribution was found to be predominantly photoelectric although a small photomagnetic contribution was not ruled out. The result indicated a cross section of about 10×10^{-28} cm^2.

In the following year Halban[29], using 450 mc of mesothorium, measured the number of photo-neutrons produced in

a 1 cm diameter sphere of D_2O at the 0° and 90° positions. The neutrons were detected by the artificial radioactivity induced in 3 gms of dysprosium oxide placed in a paraffin cone of 10° opening at a distance of 33 cm from the heavy water. The period of observation is not reported but the total number of counts obtained were 700 ± 42 at $90^\circ \pm 20^\circ$ and 47 ± 40 at $0^\circ \pm 20^\circ$. These results confirm the observation of Chadwick, Feather and Bretscher that a pure $\sin^2$ distribution would pretty well account for the intensities observed at the two positions on consideration of the geometrical conditions prevailing. Following the method of Amaldi and Fermi[30] in which the total number of neutrons slowed down in a large tank of water are counted, he finds for the total cross section $9 \pm 0.8 \times 10^{-28}$ cm^2. The contribution from the electric effect is reported as 9×10^{-28} cm^2 but the magnetic contribution, 6×10^{-29} cm^2 for an upper limit value, is much lower than that obtained using the experimental value of the capture cross section of neutrons by protons in (12).

In 1942, Myers and VanAtta[5] used a continuous spectrum of x-rays up to a maximum of 2.43 Mev to produce photo-disintegration. The apparatus consisted of a 1 cm diameter sphere of D_2O at 7.5 cm distance from the x-ray target. A sheet of silver (6.6 cm x 4.6 cm), enclosed between sheets of paraffin and located 10 cm from the D_2O, acted as the detector. The silver was activated for 3.75 minute periods and then rolled around a G-M counter. The angular distribution of the neutrons was

found to be approximately isotropic. In view of the fact that a maximum quantum energy of .25 Mev above threshold was used (the major part of the intensity fell within .10 Mev above threshold), this result should be theoretically expected. A rough estimate of the ratio of the photomagnetic to photo-electric cross section is given as 6 to 1. With still lower precision the authors estimate the total cross section at 10^{-28} cm^2 for an average taken over the continuous spectrum.

A more recent investigation designed to measure the angular distribution is that performed by Graham and Halban[25] in 1945. The apparatus consisted of a glass sphere of heavy water placed midway between two BF_3 chambers surrounded with cadmium covered paraffin cylinders. The cylinders were set at 75 cm from each other. With this geometry the neutrons coming from the heavy water were allowed a cone opening of 7.5° at the paraffin detectors. The gamma ray source, 200 mc of radio-thorium, was placed at a fixed distance from the heavy water such that the angular distribution of the gamma rays producing photo-neutrons reached up to 33°. Measurements were made with two spheres of 7.7 mm and 16 mm diameter with fixed distances from the gamma ray source of 1 cm and 2 cm, respectively. The angular distribution measurements were made, using the two detectors simultaneously, at angles of 0°, 45°, 90°, 135° and 180° by rotation of the radio-thorium about the heavy water sphere. Due to the relatively low intensity yield of neutrons from this geometry, an attempt

was made to minimize error due to statistical fluctuations by taking measurements lasting over 8 to 10 hour periods. At best the true number of neutron counts per minute at the 0° and 90° positions was 1.13 and 2.72, respectively, using the larger heavy water sphere. Corrections were found necessary for geometrical conditions, scattering by the room, and scattering by the heavy water. By using the value of the total cross section (10×10^{-28} cm^2) published by Halban in 1938, these authors find $\sigma_m = 2.8 \times 10^{-28}$ cm^2 and $\sigma_{el} = 7.2 \times 10^{-28}$ cm^2. These values are to be compared with the calculated values using equations (6) and (12) for 2.62 Mev gamma rays, namely $\sigma_m = 3.4 \times 10^{-28}$ cm^2 and $\sigma_{el} = 12.31 \times 10^{-28}$ cm^2. Assuming the process may be described by an equation of the form $n = a + b \sin^2\gamma$, where n is the number of protons emitted per unit solid angle in a direction making an angle, γ, with the incident gamma rays, and a and b are constants, these authors find for a/b the value 0.26 ± 0.08

During the concluding weeks of the current investigation, two brief articles have appeared in the literature giving the results of recent experiments designed to measure the angular distribution of the nucleons produced by the photo-disintegration of the deuteron. In each case only preliminary results are reported; a more detailed account of the work has been delayed by the authors for publication at a later date. This fact renders a careful analysis of the techniques impossible at

---

* The value of $\sigma_m = 3.9 \times 10^{-28}$ cm^2, as reported by these authors, was incorrectly evaluated; the correct value should have been that given above.

the present time. Nevertheless, analytical comparisons may be drawn between the numerical results of the current investigation and those recently reported.

In a letter to the editor of the Physical Review, dated December 15, 1948, Lassen[31] at the University of Copenhagen reports the results obtained in the angular distribution measurements of photo-protons using Na^{24} gamma rays. A battery of parallel proportional counters filled with deuterium was irradiated with gamma rays from 500 mc of sodium. Protons, created in the gas and directed approximately parallel to the counter axes, gave rise to larger pulses than those traversing the counter axes at large angles. At a given counter orientation with respect to the gamma rays, the pulse size distribution curve falls off with increasing pulse sizes; near the end, however, a peak occurs whose height is proportional to the number of pulses of maximum size. The proton paths corresponding to the peaks are those traversing the counters lengthwise but contained within an angle whose magnitude is determined by the range and counter diameter. This angular opening and that of the gamma rays is not reported. By rotation of the counter axes with respect to the gamma ray direction, the angular distribution could be investigated. The accuracy attending this method is greatly limited by the large statistical variation in the number of protons recorded at the smaller ϑ-angles. This fact is evident

by the spread in the angular distribution data shown plotted in the published letter. Lassen reports for a/b the value 0.22 ± 0.04. This gives for the ratio of the total cross sections the value $\sigma_m / \sigma_{el} = 0.33$.

In January, 1949, Hamermesh and Wattenberg[32] announced the results of preliminary measurements on the angular distribution of photo-neutrons using 40 curies of radio-sodium prepared in the Argonne nuclear reactor. The account of this work is briefly reported in abstract form in the January Bulletin of the American Physical Society. The geometrical arrangement of the apparatus was very similar to that of Graham and Halban mentioned above. The angular openings of the neutrons and gamma rays measured at the D_2O position were approximately 9° each. The work reported was performed indoors and necessitated approximately a 20% correction* for neutron scattering by the walls. Further details regarding scattering by the heavy water, statistical errors in measurement, total neutrons detected, etc. are not reported. The preliminary value of a/b = 0.24 first announced in the Bulletin was later revised downward to the value a/b = 0.15 $\pm$ 0.04 presumably due to application of a scattering correction. The several corrections to the data are being subjected to further investigation by these authors.

B. Discussion of Present Method

From the historical summary presented above, we have seen that previous attempts to investigate the angular distri-

*Private communication

bution of neutrons or protons arising from the photo-disintegration of the deuteron have in general been handicapped by low intensity measurements. On the one hand, cloud chamber experiments have failed to yield reliable results because of the small number of photo-proton tracks observed. The results of such experiments have led to the conclusion that the angular distribution is predominantly photoelectric and hence conforms to a $\sin^2$ law - a result which is in contradiction with theory. On the other hand, methods using detectors either in the form of counters or of activated foils have indicated the presence of a photomagnetic component to the total cross section. However, here quantitative agreement between the several authors is in general lacking with the result that an experimental verification or denial of existing theory is not adequately provided.

Experimenters employing the second method above have used relatively poor geometry in the experimental arrangement of the apparatus. Ideally, it is, of course, desirable to have the angle between the primary gamma rays and the observed photo-neutrons as well defined as possible. For this condition to prevail, the solid angle defined by the detector at the heavy water position, and the solid angle defined by the heavy water at the source position should both be small. These criteria, however, were sacrificed largely in an effort to gain intensity.

The method to be reported here is an attempt toward a more satisfactory investigation of the angular distribution

of the photo-neutrons. An experimental arrangement was selected in which the geometrical conditions were such as to give improved definition of angle while at the same time providing a higher intensity photo-neutron yield. The total angular spread allowed the neutrons and the gamma rays was approximately 12°. This is 33% smaller than any opening heretofore used.

In addition to the advantages derived by choice of geometry, several other features have been incorporated which are designed to enhance the measured neutron yield and to reduce the number of corrections otherwise necessitated. Among these we may mention (a) the use of BF_3 gas enriched in B^{10} to increase the counter efficiency by a factor of five, (b) the use of relatively strong gamma ray sources, (c) the elimination of the photo-neutron background due to wall scattering, and (d) the reduction of the photo-neutron scattering effect produced by the heavy water. All together, these improvements in the technique and conduct of the experiment serve a threefold purpose.

(1) They simplify the interpretation of the data by eliminating the need for corrections whose amounts are difficult to estimate

(2) They permit the conclusion that essentially all of the intensity recorded by the detector is caused by undeflected neutrons coming directly from the heavy water

(3) They produce a higher intensity of detected photo-neutrons than heretofore obtained and thereby a smaller error from statistical fluctuations.

Prior to the start of the present investigation, all experiments using counters as the means of detection have been performed with gamma rays of 2.62 Mev or less. Richardson and Emo[28] used the harder gamma rays from Na^{24} but their low intensity cloud chamber study of the photo-protons did not allow final conclusion on the existence of the magnetic photoeffect. At the higher energies the contribution of the magnetic effect should be of less importance than the electric effect. However, the theoretical value predicted by equation (8), or (12), should lie well within the range of experimental detection. In view of this fact, it seemed desirable to repeat the measurements using the 2.76 Mev gamma rays from Na^{24}. With the advantages in technique described above, the object of this investigation was a more reliable determination of the angular neutron distribution at the specified gamma ray energy. From this result it was hoped that an experimental check would be provided on the relative contribution of the magnetic and electric effects to the total cross section as predicted by theory.

CHAPTER IV

EXPERIMENTAL APPARATUS

A. Auxiliary Electronic Apparatus

1. General:

In the use of a proportional counter, the discharge produces a voltage pulse on the central wire system which may be quite small and may require considerable amplification. A pulse of 10^{-4} volt is not uncommon from such a counter. Therefore, a high gain circuit will be required to amplify such a pulse so as to allow operation of recording apparatus.

For this investigation, a general purpose linear amplifier was constructed following the design developed by Jordan and Bell[33,34]. Its function is to receive signals from, and supply power to, a preamplifier to which the counter is connected. After the signals are differentiated and amplified, they are allowed to pass through a discriminator or pulse height selector (PHS) so that only pulses larger than a selected value will be counted by the scaler. The latter apparatus then drives a mechanical counter.

A high or low level output from the video amplifier permits visual observation of the pulses on an oscilloscope thereby affording a means of monitoring during the counting process. Voltage for the counter is derived from a separate

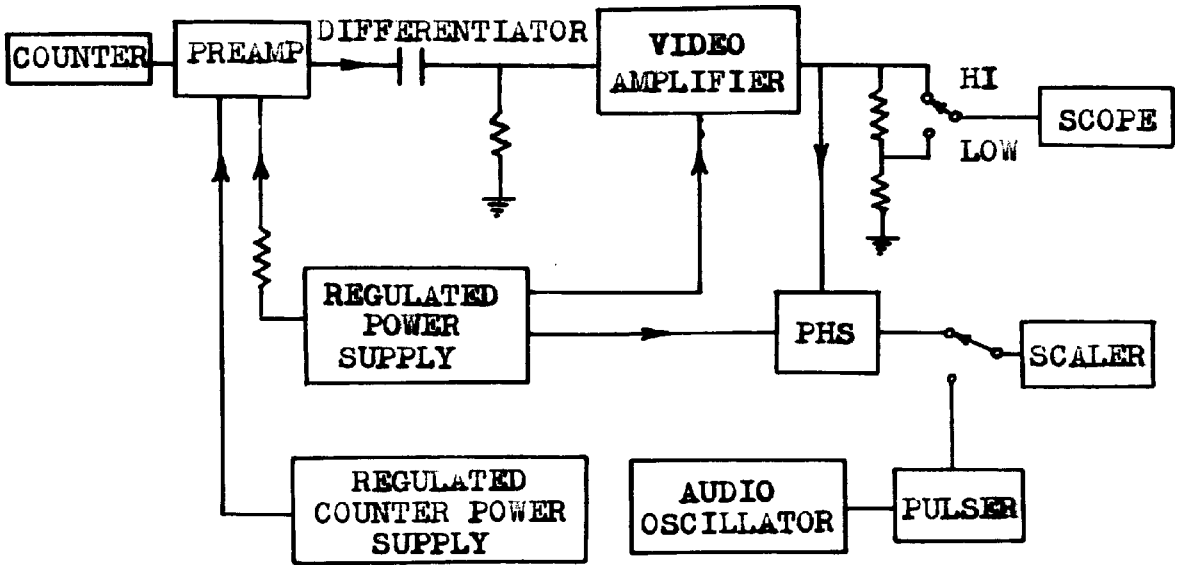

BLOCK DIAGRAM

FIGURE 1

regulated power supply capable of delivering continuously variable voltages from 1000 to 3200 volts. A block diagram of the apparatus is shown in Figure 1.

The differentiator, video amplifier, pulse height selector and power supply are included on the main amplifier chassis. The audio-oscillator and pulser served as auxiliary means for periodically testing the scaling circuit. Such testing was performed before each experimental run to guarantee satisfactory performance and consistency of operation of this portion of the apparatus.

2. Main Amplifier

The main amplifier consists of three distinct parts: the video amplifier proper, the pulse height selector, and the

regulated power supply. Input signals are differentiated by one of three possible R-C networks the selection of which permits choice of time constants of approximately 0.2, 2.0, and 20 microseconds. By choosing time constants which are much shorter than other coupling time constants in the amplifier, the output pulse is essentially free from overshoot. Other advantages of this choice include: rapid recovery times to permit high counting rate experiments, reduction in microphonics and hum, and toleration of much larger beta-ray background when counting alpha particles.

The video amplifier consists of two cascaded feedback sections and a cathode follower output tube. Each section has two gain stages and a cathode follower. By employing degenerative feedback from cathode to cathode, the gain is stabilized and an improvement in linearity is realized. The high frequency cut-off of the amplifier is variable allowing selection of frequency cut-offs of 2.0, 0.5, and 0.1 Mc/sec. As this band switch is ganged to the differentiation switch, the wide band position gives the shortest pulses at the output with a gain of 100 in each section. These shortest pulses are difficult to observe on an ordinary scope. The narrow band position gives the best signal to noise ratio. Here the gain of the second section is 100, while the gain of the first section is greater than 100 in the medium and narrow bandwidth positions.

The overall gain may be varied stepwise by factors of two - the maximum gain being the 64 position. Continuous con-

trol of gain between steps is also provided on the front panel. Using reduced gain setting the amplifier frequency response has been investigated using a Boonton beat frequency oscillator, Type 140-A, to provide variable frequency input of known voltage; the output was measured on a General Radio Company vacuum tube voltmeter, Type 726-A. Graph No. 1 shows the resulting voltage amplification plotted against logarithm of the frequency for each of the three band widths.

The input pulse to the amplifier or preamplifier may be of either sign; however, the amplifier delivers only positive pulses.

A high or low level output switch is provided on the front panel. The high impedance position is used for direct scope deflection in which positive signals up to 100 volts are obtained. In the low position a maximum pulse size of 5 volts is available requiring the use of a broad-band amplifier at the scope. The latter position is employed when fast counting speeds are desired; the pulse rise time is about 0.2 microseconds. In these tests a Du Mont 224-A oscilloscope was used simultaneously with the scaler during the counting operation.

A pulse height selector is included in the amplifier chassis. Its function is to pass only those pulses which are larger than a selected value. With the aid of a calibrated dial, pulses between 0 and 100 volts may be measured with an accuracy of $\pm$ 0.5 volts. This dial operates a potentiometer which sets a bias on a 6AK5 amplifier tube. Any pulse exceeding

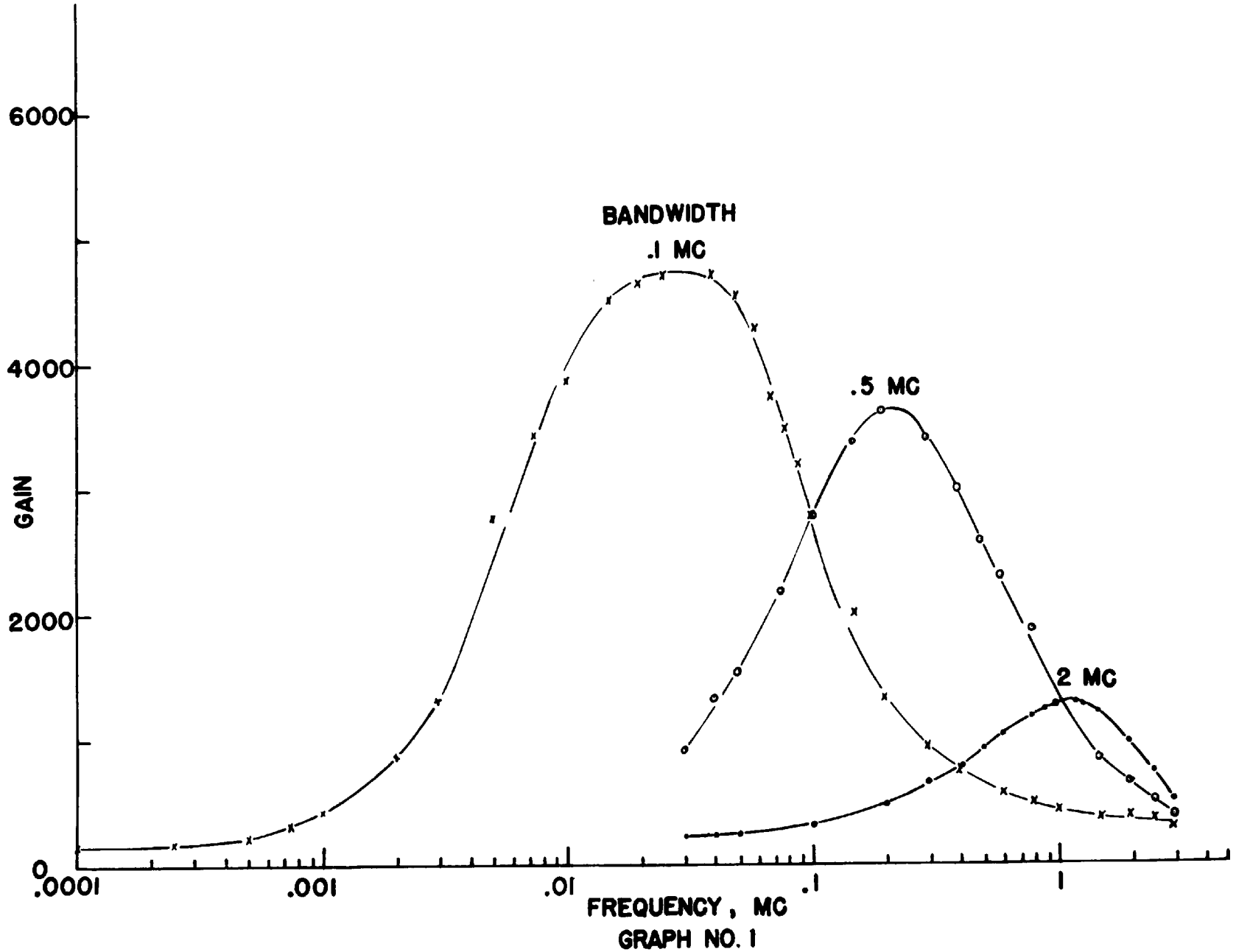
6000
4000
2000
0
GAIN
BANDWIDTH
.1 MC
.5 MC
2 MC
.0001
.001
.01
.1
1
FREQUENCY, MC

GRAPH NO. 1

this bias is amplified and triggers a multi-vibrator whose output is then differentiated and applied to the grid of an output tube. Here, the negative pulse from the differentiator is clipped. The output of the pulse height selector is a positive pulse 3 volts in height and of 0.4 microseconds duration. This output drives the scaler by means of a coaxial cable.

The approximate linearity of the input cut-off voltage with PHS dial setting is shown in Graph No. 2. These data were taken using an input signal of 70 kc from a square wave generator having calibrated output voltage. The linear amplifier band width was set at .1 Mc/sec. The PHS dial setting just sufficient to produce cut-off was determined by visual observation on an oscilloscope. At cut-off the sharp pulses corresponding to the differentiated and amplified square waves were seen to disappear sharply.

The power supply for the main amplifier is electronically regulated and of standard circuit design for operation from a 115 volt, 60 cycle line. The amplifier gain is independent of reasonable line voltage fluctuations. However if the line voltage falls below 107 volts, the electronic regulator will not function properly. A regulated $\pm$ 260 volts is available from this circuit; lower voltages for operating some of the stages is obtained by voltage-dropping resistors.

3. Preamplifier

The linear amplifier described above is designed to be used with a preamplifier[34]. However, in the present instance

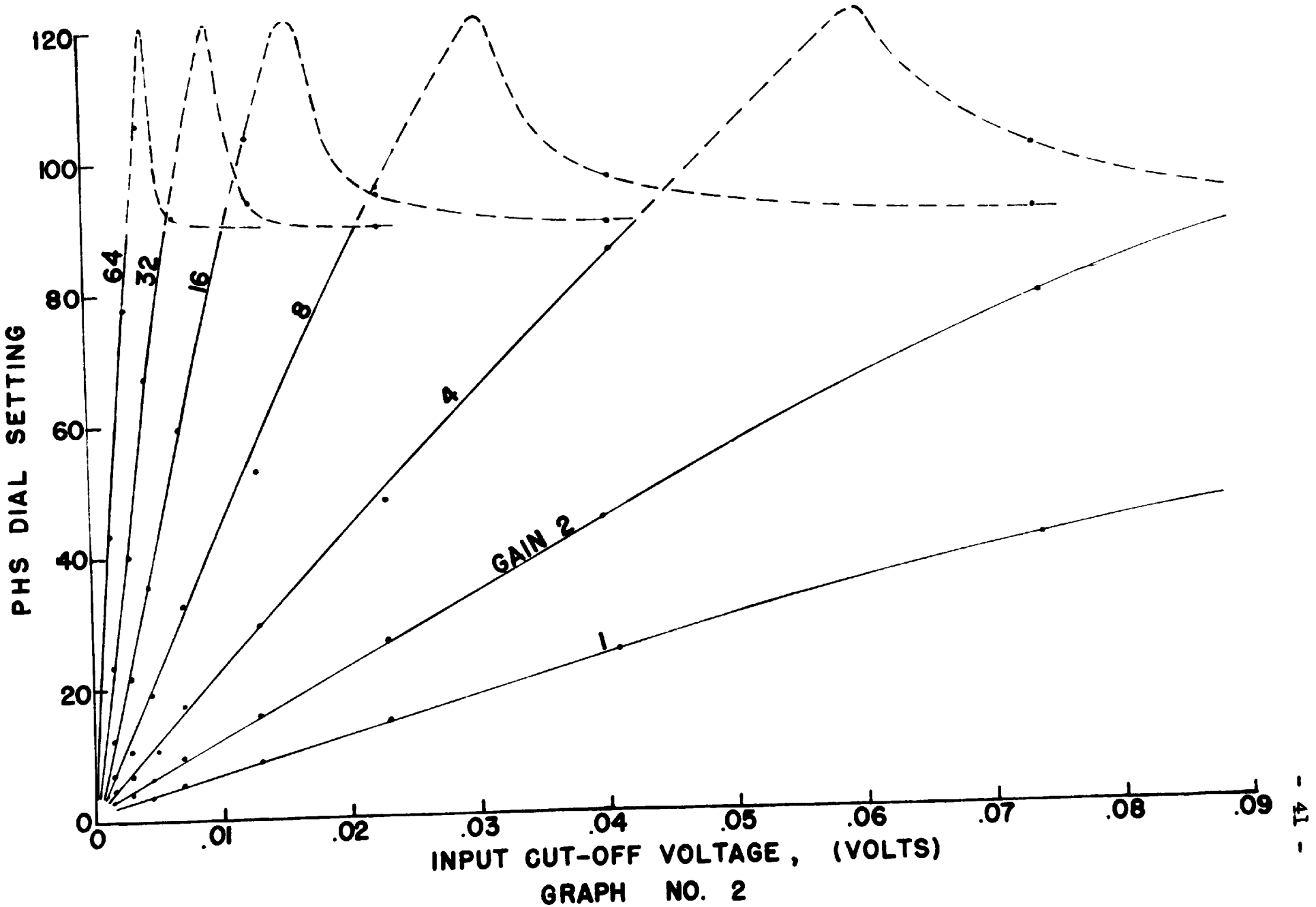
120
100
80
60
40
20
0
PHS DIAL SETTING
64
32
16
8
4
GAIN 2
1
0
.01
.02
.03
.04
.05
.06
.07
.08
.09
INPUT CUT-OFF VOLTAGE, (VOLTS)

GRAPH NO. 2

gain from the preamplifier is not necessary when a proportional counter is to be used. For this reason a single stage preamplifier, which is nothing more than a cathode follower with gain slightly less than unity, is suitable. A 6AK5 tube serves for this purpose very satisfactorily.

To reduce extraneous counts, extreme caution must be exercised in the construction of this stage. As the high voltage for the counter is coupled to the input grid of the preamplifier tube, all circuit elements here must be carefully selected. For example, the coupling and filter condensers must be good insulators and must have high leakage resistance. To withstand the high voltage, mica condensers of 5000 volts test rating were used. The 20 megohm grid leak and counter voltage resistors were of the metalized type specifically selected for their noise-free operation. These circuit elements, along with the stand-off insulators and connector insulators at the input of the preamplifier, were carefully cleaned with carbon tetrachloride and alcohol and then coated with ceresin wax in accordance with standard practice. This procedure minimizes surface leakage by the removal of conducting surface films and by preventing the formation of slightly conducting layers of water condensed from the atmosphere. An additional guarantee against condensation which proved of considerable value was the use of a small heating element enclosed in the preamplifier chassis. This was operated off the filament power circuit and served to reduce the relative humidity within the enclosed volume.

The whole preamplifier circuit was enclosed in a tight metal box for shielding purposes. Ground return lines were kept as separate conductors so that cable and chassis shielding did not serve as current-carrying conductors. The counter was solidly connected to the preamplifier chassis and all cable connectors between components were tightly fastened in place.

One additional precaution taken was the use of a metal partition within the preamplifier box which served to shield the high voltage elements against possible pick-up from parts of the cathode follower circuit.

4. Scaler

As is customary in the use of counters, a scaling circuit was used for the purpose of reducing by a known factor the actual number of counts registered on a mechanical recorder. This practice is useful when the counting rate exceeds the rate at which the mechanical recorder can operate. Further, it improves the statistics by eliminating the possibility of having closely spaced counts register as a single count by the comparatively slow recorder.

The general principle of the scaling circuit used is that embodied in the Eccles-Jordan[35] trigger circuit. The basic unit is a trigger pair, an arrangement of two 6N7 triodes, having a characteristic curve in which a portion exhibits a negative slope. This negative slope portion is unstable thus allowing a sudden change from one stable state to another on

the application of a positive pulse to both grids. The tube which was formerly in a conducting state becomes non-conducting while the non-conducting tube will become conducting. The circuit remains in this new stable condition until the arrival of the next pulse. The two tubes alternately change roles. Any trigger pair following this unit will receive alternative positive and negative pulses and respond similarly.

In the present scaler, four such stages are used to form a scale-of-sixteen circuit. By the use of a neon lamp across a portion of one plate resistor in each trigger pair, it is possible to tell whether one or two pulses have been received by this pair. With all stages so equipped, interpolation to fewer counts than sixteen is readily made by observing which lamps are lighted. On each total count of sixteen, the output of the scaler records as a single count on a Cenco Impulse Counter.

In consideration of the relatively low intensities encountered in the photo-neutron experiments reported below, a scale-of-sixteen circuit amply reduced the operation of the mechanical recorder to a counting frequency which it could readily follow.

5. Counter Power Supply

The voltage applied to the counter maintains the central wire positive and the cylinder negative. As the cylinder also serves as the external envelope, it is desirable to operate

this at ground potential so as to permit safe handling. In addition, this arrangement provides electrostatic shielding for the central wire.

Generally, counters filled with polyatomic gases have higher starting potentials than those using noble gases. The starting potentials of mixtures will, in general, lie between those of the constituents. In consequence of the addition of 10% of argon to the BF_3 gas, the operating potential was held down to a value of the order of 2100 volts.

To provide the voltage for the counter, a power supply is required whose output is constant with varying load and is free from cyclic variations or ripples. One solution to this requirement is the use of a voltage-regulated electronic power supply. The stabilization of output voltage is accomplished by placing a variable impedance device, or stabilizer, between the filter output and the load. The impedance of the stabilizer is controlled by the output voltage so as to hold that voltage constant automatically[36]. This device will maintain constant load voltage by absorbing a varying amount of output filter voltage or input voltage to the stabilizer.

In particular, the degenerative amplifier type of stabilizer[37] was employed. This functions for changes in both input and output voltages. The load resistance was placed between the cathode of an HK24 triode and the negative lead. Grid bias was provided by a VR150 glow tube. An amplifier tube, also an HK24, was added to improve the stabilization. The regulated output voltage was continuously variable from 1000 to 3200 volts.

B. Boron Trifluoride Proportional Counter

1. Principles of Operation

a. Proportional Counters

In 1928, Geiger and Klemperer[38] laid the foundation for the modern technique of "proportional counting" whereby the difference in the ionization produced by different types of particles traversing a counter is made the basis for distinguishing between them.

When the voltage of the counter is raised above that limit, V_o, at which secondary electrons are first formed by collision, then additional ions will be formed in the neighborhood of the central wire where the electric field is greatest. The process is cumulative, giving rise to a Townsend avalanche of electrons.

The voltage, V_o, may then be defined as the threshold voltage for proportional counter action. Below this voltage, no gas amplification occurs and the number of ions collected on the central wire will be equal to the number produced in the initial ionizing event. For voltages greater than V_o, the number of ion-pairs, A, formed by collision as each electron travels toward the central wire varies from unity, when the counter acts like an ionization chamber, to about 10^7 at the beginning of the "Geiger region." Within a portion of this voltage range, A remains a constant, and the counter produces a pulse, dV, which is proportional to the number of

ions, n, formed in the initial ionizing event. This is the so called "proportional region." The voltage pulse appearing on the central wire is given by

$$dV = A\, dq/C = A\, ne/C \qquad (16)$$

where e is the charge on the electron in microcoulombs and C is the distributed capacity of the central wire system in microfarads.

By the operation of a counter in the proportional region, it is possible to distinguish between the arrival of a beta-ray and an alpha particle since there is a large difference in the total ionization produced by each of these two entities. In this fashion a device is provided which, upon selectively discriminating against the smaller beta pulses, permits the detection of the heavier ionizing alpha particles alone.

Such a proportional counter action is used in the present investigation. A discriminator is set to block out the smaller beta pulses originating from the absorption of the gamma rays while the larger alpha particle pulses resulting from the capture of slow neutrons by B^{10} are free to register on the counter.

b. Neutron Counters

Neutron counters can be built to detect preferentially either fast or slow neutrons, and can therefore be used to measure the intensity of a neutron source, the number of

neutrons in any given experimental arrangement, or the number diffusing out from some apparatus into the surrounding room.

To detect slow neutrons, a counter filled with BF_3 gas may be used. The operation of such a counter constitutes an example in which a "primary" radiation (the neutrons) in its passage through matter gives rise to a secondary radiation (alpha particles) of a different nature. The reaction involved is

$$_5B^{10} \; (_0n^1, \; _2He^4) \; _3Li^7 \qquad (17)$$

for which the cross section for slow neutron capture is 550×10^{-24} cm^2 when a normal isotopic mixture of B^{10} and B^{11} is used. For boron trifluoride consisting almost entirely of B^{10}, an increase in detection sensitivity is realized by virtue of the fact that the slow neutron cross section for the B^{10} isotope alone[39] is 3500×10^{-24} cm^2. The above reaction proceeds only for the B^{10} isotope; so the more common B^{11} isotope serves no useful purpose.

We thus see that the instrument is sensitive not to the slow neutrons, but to the secondary heavy ionizing alpha particles.

The reaction above results in the liberation of about 2.5 Mev of energy, which appears as kinetic energy of the product nuclei. Through conservation of momentum, it may be shown that the alpha particle carries about 1.6 Mev of energy and the recoiling lithium nucleus takes the balance of 0.9 Mev.

Taking 30 ev as the approximate loss of energy in the formation of each ion-pair, an evolution of 2.5 Mev in a single capture process gives rise to the production of about 83,000 ion-pairs in the counter.

It is well to note here that, while two particles are formed on the disintegration of the boron, these travel in opposite directions. Thus, if one hits the counter wall, the other travels out into the gas. The pulse so formed will be smaller than if both particles had terminated their range in the gas. Nevertheless, if only one component is effective, the amount of ionization is still considerably larger than that produced by a beta particle.

c. Self-quenching Counters

The BF_3 counter constitutes an example of a self-quenching counter wherein the presence of a polyatomic gas causes the counter discharge to terminate due to an internal mechanism. As pointed out by C. G. and D. D. Montgomery[40] and Stever[41], the secondary electrons, ejected from the counter walls by the arrival of the positive ions formed in the avalanche, cause the discharge to continue indefinitely in the case of the non-self-quenching counter. However, in the self-quenching counter these secondary electrons are absent. Korff and Present[42] have proposed a mechanism which explains this absence in a counter containing polyatomic gas molecules. Firstly, they have shown one type of quenching results from the fact

that the photons, formed in the initial avalanche, are absorbed by the polyatomic molecules which in turn predissociate before they have a chance to lose the absorbed energy by radiation. Secondly, a quenching of the secondary electron emission takes place when the positive ions reach the cathode. A detailed analysis[43] of the action taking place near the cathode wall shows that, unlike diatomic ions, the polyatomic ions are neutralized before reaching the wall and no secondary electron emission can occur. Instead of radiating, the molecule decomposes upon neutralization. The discharge cycle is not repeated to form a series of self-perpetuating avalanches. Still another source of quenching is that relating to the mobility of the positive ion space charge which in turn determines the dead and recovery times. Immediately after the formation of the electron avalanche, the positive ion sheath alters the field conditions in the neighborhood of the central wire. The electrostatic field between sheath and wire is greatly reduced and may reach such a value that no further avalanches can occur. The discharge is thus quenched and will remain so as long as no additional electrons are formed by subsequent processes such as the two mentioned above. The anode then is free to recover to its normal operating potential where it will be sensitive to the next ionizing event.

d. Counter Efficiency

If we define the efficiency, Eff., of a neutron counter as the probability that a neutron, on passing through the counter,

will be captured and detected according to process (17) then

$$\text{Eff.} = L\, p\, \sigma\, d$$

where L is the Loschmidt number, p the pressure in atmospheres, σ the capture cross section at a specified velocity, and d the average neutron path length through the counter.

To a sufficient degree of approximation we may take the average path length as equal to the counter diameter of 3.8 cm. With a counter pressure of one-third atmosphere and for enriched BF_3, we find for the efficiency of the counter employed in this investigation,

$$\text{Eff.} = 12\%$$

It is apparent that an increase in efficiency may be realized by using higher pressures; however, a practical limit is set by the fact that higher pressures require high operating voltages - an effect tending to increase the probability of extraneous counts. Of even greater importance is the fact that the beta-ray pulses become greater with increasing pressure. Both these effects tend to decrease the neutron to background ratio. In view of the small number of neutrons available for angular distribution measurement in the current investigation, it was desirable to make this ratio as large as practical without undue sacrifice in efficiency. Toward this end, a BF_3 pressure of 25 cm of mercury was selected. Since argon has a considerably lower starting potential than BF_3, it was possible

to lower the starting potential somewhat by the addition of ten percent argon to the counter. The efficiency for neutron detection depends only upon the amount of BF_3 present, and is not altered by the addition of argon.

Similar considerations served to determine the counter dimensions. A counter of larger diameter again would have required larger operating voltages. Further, a longer counter would make no change in efficiency, although the total number of counts recorded would increase. This could serve no useful purpose as the counter length was determined by the angular resolution of 5° assigned to the neutron beam. (see Figure 2, below)

Since the capture cross section of neutrons decreases according to the 1/v law, it is evident that the counter efficiency will depend upon the neutron velocity. Hence the fraction of the flux of neutrons which produces counts will depend upon the arrangement of scattering and "slowing down" material around the counter. Neutrons issuing from the photo-disintegration of the deuteron when irradiated by the 2.76 Mev gamma rays from Na^{24} have a monochromatic energy of $E_n = .29$ Mev. Since process (17) operates for slow neutrons, it is necessary, by use of some moderator such as paraffin to slow down the neutrons to near thermal energies, $E_o = 25 \times 10^{-9}$ Mev, before reaching the counter. In the moderator the mean free path of the neutrons decreases from a few centimeters at the higher energies to a few millimeters at the thermal

velocity of 2200 meters per second. The energy loss in a collision depends upon the angle of deflection. If the initial neutron energy is E_n, then the average energy after n collisions will be E_n/e^n. Thus, approximately sixteen collisions are necessary to reduce the photo-neutrons to thermal energy.

Experimentally, the optimum paraffin thickness necessary for maximum counting efficiency was found by irradiating 25 cc of D_2O with gamma rays from radio-sodium. The BF_3 counter was placed at a distance of 15 cm from this source; and the number of neutron counts was recorded in turn as 1 cm slabs of paraffin were interposed. Graph No. 3 shows the result. The large statistical variation in the number of counts recorded per minute results from the fact that for each thickness observations were made which lasted only five minutes and also from the fact that a low intensity photo-neutron source was used. However, the data served to indicate that an optimum paraffin thickness of approximately 5.5 cm should be selected for maximum counting efficiency. The general character of the observed response with moderator thickness is similar to that reported by Amaldi and Fermi for the spacial distribution of neutrons in a spherical shell of varying radius surrounding the source[44].

Guided by the above result, a paraffin form was constructed such that the front portion facing the neutron source was cylindrical in shape with axis parallel to the counter axis and of 5.5 cm paraffin thickness while the rear portion was a

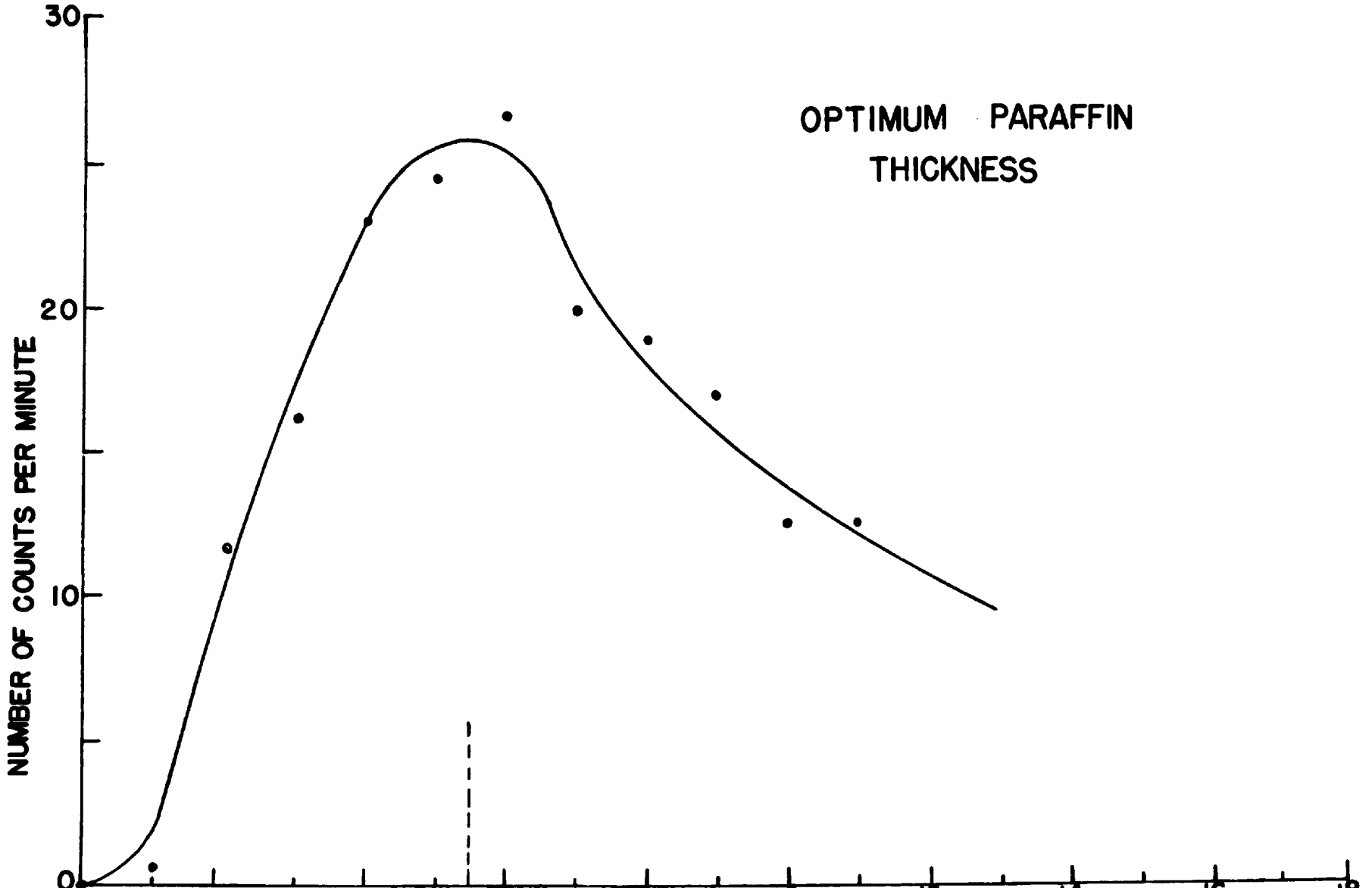
OPTIMUM PARAFFIN
THICKNESS
NUMBER OF COUNTS PER MINUTE
30
20
10
0
0
2
4
6
8
10
12
14
16
18
PARAFFIN THICKNESS, CM.

GRAPH NO. 3

hemisphere of 15.5 cm diameter. For purposes of symmetry, the front cylindrical portion was then machined so as to present a circular view of 15.5 cm diameter to the neutron source. (see Figure 2)

Preliminary tests showed that an increase by a factory of approximately four or five in the number of counts recorded could be gained by orienting the cylindrical counter so as to present a side view instead of an end view to the incident neutron beam. The solid angle subtended by the moderator at the source for each of the two orientations was maintained approximately the same in this test.

e. Counter Background

All counters exhibit background to a greater or less degree. It is the statistical fluctuation in this background which sets the final limit to the smallest amount of ionization detectable by a given instrument.

In general we may attribute background to two causes: the first of these is in the nature of radiation arising from sources other than that under investigation; the second has its source in the electronic circuits and mechanical devices used in amplifying and recording the ionizing events. By suitable precautions in construction and by the application of established techniques, each of these sources of background may be reduced to a minimum. However, in the limit some background will always be present.

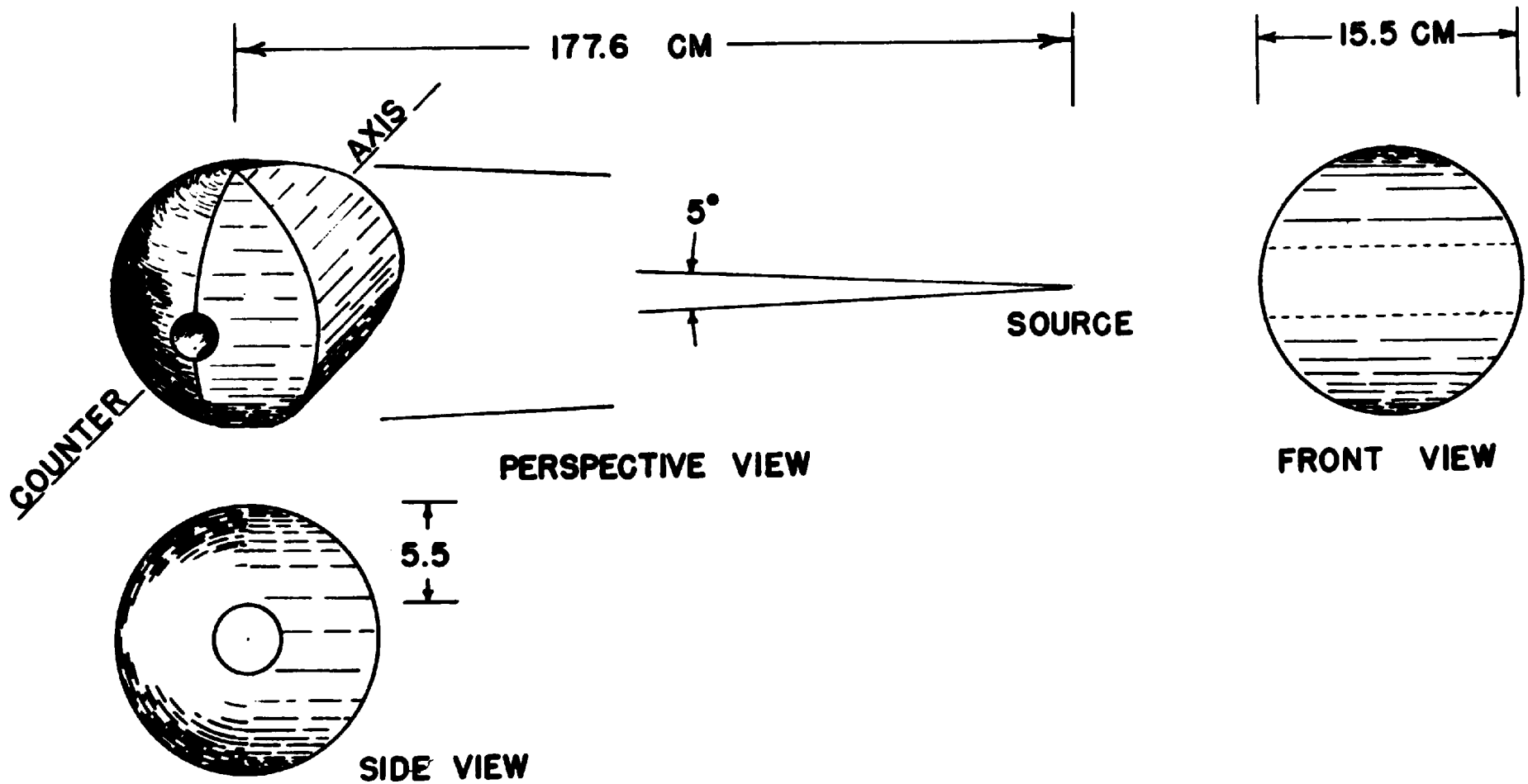

PARAFFIN MODERATOR

FIGURE 2

Background due to radiation: This is caused by three types of radiation; (a) alpha particle contamination of the inside of the chamber, (b) cosmic radiation, and (c) natural radioactivity of the surroundings. No special precaution was taken in the elimination of alpha particle contamination other than the selection of brass stock for the cathode which had not been stored in the neighborhood of a cyclotron or of any known radioactive sources. It was possible throughout the tests to use a discriminator setting high enough to exclude a large share of the background arising from radiation sources (b) and (c) without reducing the number of photo-neutrons counted. This condition surely prevailed for background events which produced pulses much smaller in size than those due to the heavily ionizing alpha particles originating from neutron capture by B^{10}. Evidence confirming this is found in the fact that normally background amounted to approximately one count per minute whereas about 1.5 cosmic rays per minute can be expected to cross every square centimeter of horizontal cross sectional area of the counter at sea level.

Background of mechanical and electrical origin: Extraneous counts are not uncommon with apparatus designed to amplify small pulses from ionization chambers, proportional counters, or similar devices, to a level where the pulses can be seen on an oscilloscope and counted with a scaler. A common source of such counts is breakdown of insulators, particularly those at the input of the preamplifier where high voltages are applied.

To minimize this, all elements such as the ceramic coupling condenser to the preamplifier grid, the grid leak resistor and T-filter elements, the insulators in the connectors, and stand-off insulators supporting the anode leads were carefully cleaned with alcohol and coated with ceresin wax. These were then mounted without being touched with the fingers.

Effort was made to avoid external sources of interference by operating at night and at such times when offending pieces of equipment were not in use. Radiation pickup was minimized by having everything connected to the input grid enclosed in a tight metal shield. The shield was connected solidly to the preamplifier chassis; ideally the counter should be welded or soldered to the preamplifier, but this proved impractical. No wires or posts were permitted to project through the shield where they could serve as antennae.

The 110 volt a.c. power to the linear amplifier and counter power supply was provided through an isolating transformer designed with electrostatic shield to isolate line noises and interference.

Leads to these components from the transformer were covered with braided shielding to reduce the possibility of radiation pick-up along these lines.

The use of multiple grounds was scrupulously avoided throughout the construction of the linear amplifier, preamplifier, and associated equipment. To this end, the counter was connected only to the preamplifier, the preamplifier was then connected

only to the amplifier by the shielded power cable. Similarly, connection to other equipment such as power supply, scope, and scaler was made with equal care. Unfortunately, most of these components are already "connected" to the power line through the capacity between primary and secondary of the power transformers. The precaution to take, therefore, is to plug all the equipment into a single multiple socket.

Additional safety precautions against the possibility of extraneous counts by insulator breakdown were the addition of a small heating element in the metal preamplifier shielding box to reduce the relative humidity therein and the use of a calcium chloride dehumidifier in the shielding cup at the far end of the counter.

Counters are often sensitive to microphonic disturbances. These effects are often traceable to the fact that components of the apparatus move relative to one another causing changes in the capacity of the system. The practical approach to the solution of this problem is to construct the components with rigidly mounted parts and to provide vibration-free supports wherever practicable. Such practice was adhered to where possible. The counter anode for example was mounted without the use of the customary phosphor bronze spring. Instead, the three mil tungsten wire was sealed to the glass counter ends while under tension thus providing a taut filamental structure.

In the event negative ions are formed within the active volume of the counter during the discharge, a longer time will

be required for their passage to the anode than that required by the more mobile electrons. These ions may arrive in the high field region near the wire after the Townsend avalanche is over and after the positive ion space charge sheath has progressed far enough to permit restoration of the field near the wire to normal value. In this case the negative ion may lose its electron by action of the high field in the neighborhood of the wire. This electron is then free to start a new avalanche and produce a count. Similarly, the negative ion may produce ionization by collision and thus start a new Townsend avalanche. In this way spurious or multiple counts may be produced. To prevent such an occurrence, special care must be exercised to eliminate from the chamber those gases having low enough electron attachment coefficients to produce significant effects. Of these, oxygen and water vapor may be mentioned. Toward this end particular effort was made in the evacuating and filling process to outgas the anode and counter cylinder thoroughly and to evacuate to a pressure of less than 10^{-6} mm of Hg before admitting dry BF_3. Also to provide a long and useful counter life, all solder seals were painted with glyptol to prevent even slight air leakage over a period of months. The details of this procedure are outlined in the next section.

In concluding this discussion on background, we should, in the interest of completeness, mention the very important role played by the photo-neutron background produced by scattering

from walls and objects surrounding the apparatus used in making the angular distribution measurements. Since the magnitude of this effect is considerable as shown by supplementary tests, we shall consider the method employed in its elimination in a later section. It is sufficient to mention here that background due to slow neutrons originating from all sources exterior to the detector was minimized by use of a ten mil thickness cadmium sheet surrounding the paraffin form.

2. Design, Construction, and Characteristics

a. General

The particular design chosen for a counter must satisfy certain specific requirements as dictated by the use to which it will be put. As examples of these requirements, we may mention the following. The type of radiation to be studied will set certain limitations upon the choice of the envelope material and of the filling gas employed. The overall dimensions of the sensitive volume will in general be prescribed by the nature of the investigation and the radiation intensity - for example, in working with weak sources, a large solid angle counter may be desirable. A low natural background for the counter is especially important when working with weak sources, and undesired radiation must be excluded when possible by proper design considerations. The techniques in design which provide for the elimination of spurious counts deserve special

attention if one is to place any trust in the true random character of the data. One must be guided also by considering the extent to which the counter efficiency depends upon counter form and dimensions. In addition to these, we may add such considerations as simplicity of construction, ruggedness of form, and adaptability to specific uses.

b. Design

An attempt was made to meet the specific requirements of the present investigation by constructing a boron trifluoride proportional counter of relatively large internal diameter and of such length as to guarantee full use of the sensitive volume as defined by the paraffin form. The envelope was constructed of cylindrical brass tubing to which brass ends were soldered for the purpose of supporting the glass anode insulators. The whole of the counter interior was thoroughly polished to guarantee removal of all burrs, scratches, and irregularities.

As the wire diameter is one factor which determines the operating voltage, a three mil tungsten wire was selected for the anode. A largerdiameter wire would have required higher voltage, while a smaller diameter wire would have been too fragile for ordinary handling.

To extend the useful lifetime of the counter all seals were permanently constructed. In the case of BF_3 counters, the gas attacks wax or rubber seals and the useful life of the

counter is correspondingly reduced. To avoid this, Kovar to glass seals were used. These permitted soldering the glass insulators to the brass cylinder ends while the anode itself was fastened by a tungsten to glass (Corning 7052) seal. Since no phosphor bronze spring was used to keep the anode taut, the glass-tungsten seal was made under tension as the last operation in the assembly.

The details of the counter design are shown in Figure 3. The long glass anode supports were specifically chosen to provide as long leakage paths as possible with considerable portions of the glass surface oriented normally to the electric field direction. The places where the anode is spot-welded to the heavier tungsten leads were shielded with glass sleeving to avoid high local fields. Such fields give rise to local ionization which results in spurious counts.

c. Cleaning and Evacuating

Prior to evacuation the counter was washed in boiling carbon tetrachloride for approximately one-half hour, then cleaned with alcohol and finally rinsed with distilled water about eight or ten times. This process is designed to remove all traces of wax, grease, and dust which would otherwise alter the operating characteristics over a period of time or cause distortion of the field and give rise to spurious counts.

To guarantee that all seals were vacuum tight, the counter was evacuated to a pressure of 10^{-6} mm of mercury. The tempo-

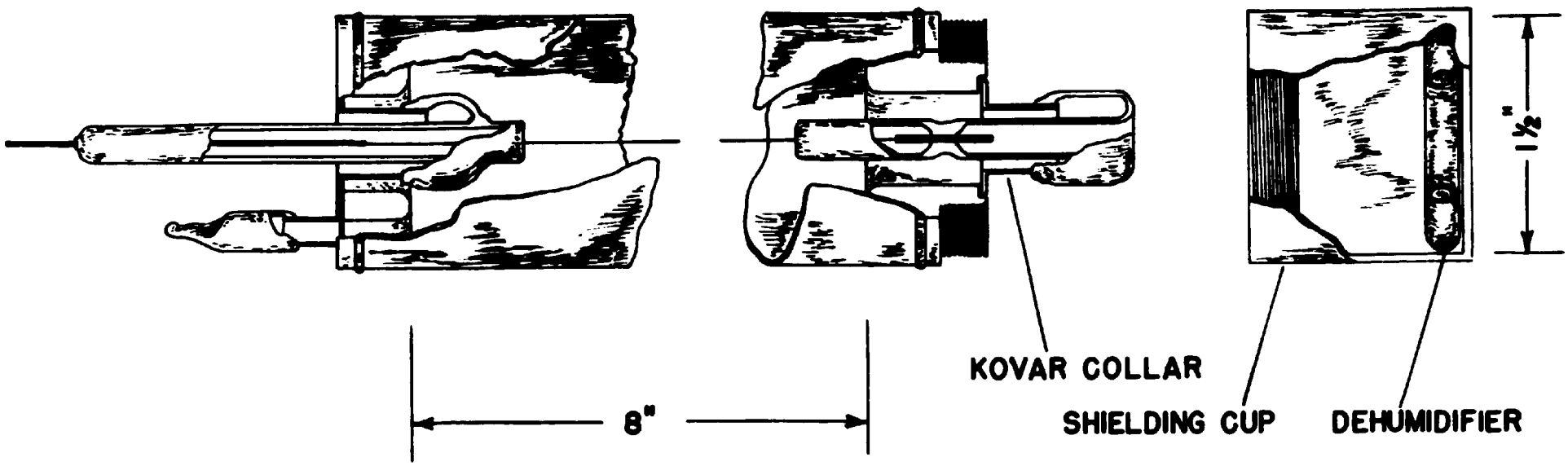

SECTIONAL VIEW OF COUNTER - FULL SCALE

FIGURE 3

rary glass stopcock on the seal-off tube was then closed and the counter was allowed to stand for three days. At the end of this time, it was again tested and found to be vacuum tight.

As a final precaution against slow leakage, all solder seals were painted with glyptol prior to the filling operation.

d. Filling Process

To fill the counter with boron trifluoride[45,46], the filling system shown in Figure 4 was assembled. The counter, mercury manometer, and condensing tube were incorporated into a compact unit on the vacuum system. In this fashion, waste volume was minimized so as to conserve on the amount of BF_3 needed to attain the desired gas pressure.

A one liter flask containing commercial argon of 99.6% purity at one-half atmosphere pressure was attached at the closed end of the system as shown. A condensing trap connected to this flask served to remove any condensible vapors which may have been present at the time of filling.

The boron trifluoride gas used in the counter is extracted from a boron trifluoride-calcium fluoride complex. As furnished by the AEC, Isotopes Branch, the boron in the complex form, $CaF_2 \cdot BF_3$, is 96% B^{10} as compared with the 20% content of B^{10} in a normal isotopic mixture.

To generate the BF_3 gas, the complex must be heated slowly in a closed, evacuated, system to a temperature of 280°C. The

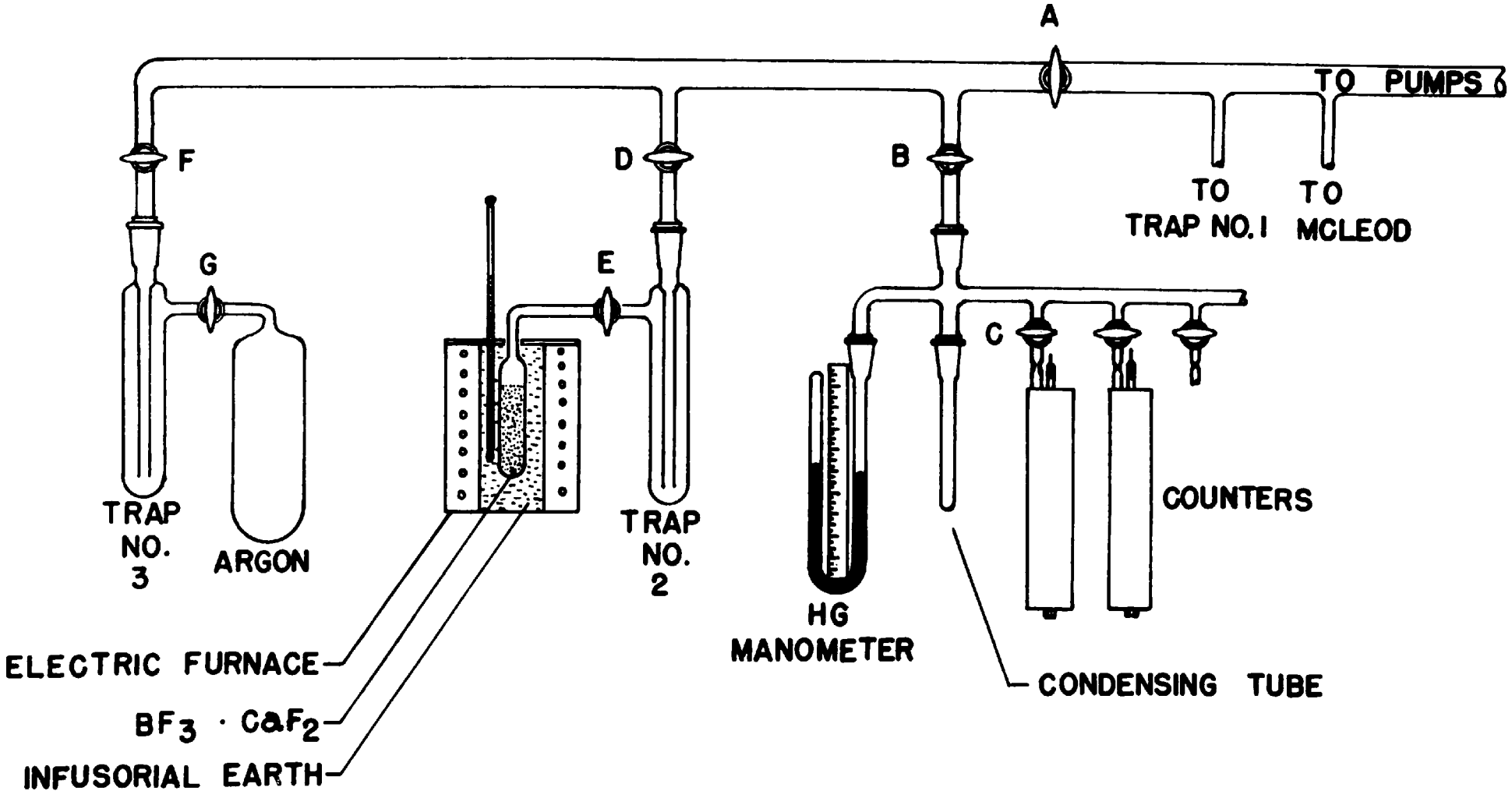

FILLING SYSTEM

FIGURE 4

generating process is simply

$$CaF_2 \cdot BF_3 \xrightarrow[\Delta\ 280^{\circ}C]{} CaF_2 \downarrow + BF_3 \uparrow$$

Ten grams of the complex in finely powdered form was placed in a glass container, then attached to the vacuum system, and surrounded by a small electric furnace. Infusorial earth was then packed around the container to provide insulation against excessive heat loss and also to assist in distributing the temperature more or less uniformly over the glass surface. This portion of the system was provided with a separate liquid air trap designated as Trap No. 2 in Figure 4.

With liquid air around Trap No. 1, the $BF_3 \cdot CaF_2$ was outgassed at room temperature for twelve hours, and then outgassed at 85°C for an equal length of time or until a pressure of 10^{-6} mm of mercury was reached. Then with stopcock D closed, the anode was glowed to a cherry red for fifteen minutes by electrically heating the 3 mil wire with the aid of a .5 k.w. Variac. This operation effectively removes dust and sharp points from the wire surface and drives off occluded gases. To further enhance the chemical stability of the counter, the metal envelope was carefully heated with a Bunsen flame at this time for the purpose of outgassing the counter wall. Caution was necessary in this operation to make certain the temperature of the metal was not raised above the melting point of the soft solder used at the seals.

The complex was next slowly heated to 280°C over a period of four hours. Liquid air was maintained around Trap No. 2 throughout this process and stopcocks A, D, and E were kept open. By closing stopcock A, removing the liquid air from Trap No. 2, and freezing the condensing tube, it was possible to draw all the BF_3 over into the manometer-counter system. Then on closing stopcock B and removing the liquid air from the condensing tube, a periodic check could be made from time to time of the amount of gas generated as indicated by the manometer.

When the desired pressure of 25 cm of mercury had been attained, the liquid air was removed from Trap No. 2 and a dry ice-acetone mix substituted immediately. This latter freezing mixture served to hold condensible vapors in Trap No. 2 while at the same time it could not maintain a low enough temperature to prevent the BF_3 gas from evaporating over into the condensing tube where it was trapped by the use of liquid air. A dry ice-acetone mixture was next placed around Trap No. 3. With stopcock A alternately closed and opened, the system was flushed two or three times with argon at a few centimeters of pressure by opening stopcocks F and G briefly. This was drawn off by the pumps after each flushing operation.

Next argon was admitted into the counter to a pressure of 2.5 cm of mercury as read on the manometer. With stopcock B closed, the BF_3 was released as a gas by removal of the

liquid air from around the condensing tube. Finally, the counters were sealed off at the glass constriction after stopcock C had been closed.

In the final preparation of the counter, all exposed glass insulator surfaces were washed in carbon tetrachloride and alcohol. These were then coated with ceresin wax by dipping into a wax bath at 100°C. The shielding cup was next screwed in place and the counter was allowed to stand several hours before testing.

From the standpoint of economy, it is advisable to prepare and fill several counters at one time. This would effect a saving in BF_3 since a certain amount of boron trifluoride is inevitably lost at each filling. A large portion, but by no means all, of the remaining BF_3 can be reabsorbed back into the cooled CaF_2. Storage of the remaining gas in a glass container offers one solution to this problem. However, since stopcock grease is eventually attacked by the gas, the storage tank must be closed by use of a mercury seal, or less desirably, by sealing off the glass connecting tube to the storage container with an oxy-gas flame.

e. Counter Characteristics

Before using the counter for any quantative measurements, it is necessary to investigate its operational characteristics. By this means we may determine whether the several desirable features sought in any counter have been realized by the choice

of design and mode of construction and filling. To list but a few of these desiderata, we may mention: (a) low operating potential, (b) long and flat voltage range or plateau, (c) large difference in pulse sizes produced by different types of ionizing particles, (d) high efficiency, and (e) stability with use and time. We consider each of these below.

To investigate the plateau curve for this proportional counter, the aforementioned auxiliary electronic equipment was used with amplifier at full gain setting, pulse height selector set at 40, and bandwidth at .1 mc/sec. As the counter is sensitive only to slow neutrons, a paraffin moderator was placed about the counter. A very weak polonium-beryllium source of fast neutrons was next placed close to and at a constant distance from the counter. With this arrangement the alpha particle counting rate as a function of counter potential was obtained as plotted in Graph No. 4. The somewhat large statistical variation displayed in the data plotted here arises from the fact that at each voltage setting observations were taken for only ten minute periods. This counting rate curve is an integral curve, in which all pulses greater than a certain size are measured. The flat plateau indicates that in this region all pulses are of a certain maximum size. Any departure from flatness would be an indication of the presence of spurious counts as could be produced by the presence of air giving rise to occasional negative ion formation. Moreover, a flat plateau is desired as it insures a counting rate independent of small

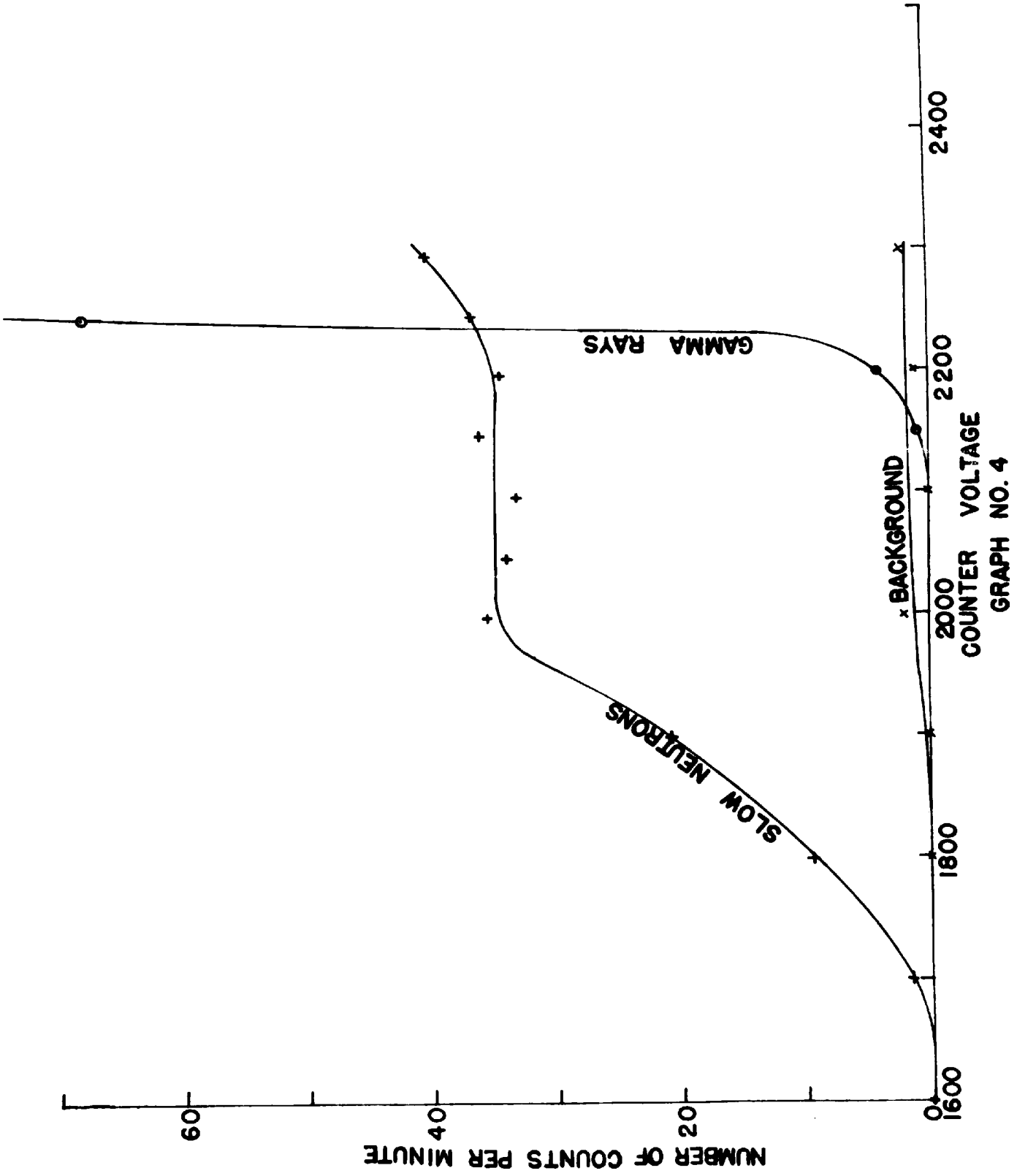
NUMBER OF COUNTS PER MINUTE
0
20
40
60
1600
1800
2000
2200
2400
COUNTER VOLTAGE
GRAPH NO. 4
BACKGROUND
GAMMA RAYS
SLOW NEUTRONS

fluctuations in operating potential when the counter is operated somewhere near the middle of the flat portion.

An investigation of background, which we may define here as those counts arising from any origin whatever in the absence of the Po-Be source, gave at most one or two counts per minute. This is shown plotted on the same graph.

To investigate the effectiveness of the pulse height selector in discriminating against smaller pulses such as those produced by beta particles, the counter was exposed to the gamma rays from a strong Co^{60} source. As can be seen from the graph, only at voltages greater than 2100 volts was the gas amplification, A, equation (16), sufficient to produce beta pulses whose magnitude exceeded the cut-off setting of the pulse height selector.

From the information derived by tests of the above type, the operating constants to be used in the angular distribution measurements were determined. For example, the operating potential selected for normal use of the proportional counter was 2100 volts. With this value, operation in the flat region of the plateau was assured. Further, the possibility of counts arising from the absorption of gamma radiation was minimized. This voltage is not unduly large when one remembers that the starting and operating potentials of self-quenching counters are in general somewhat higher than those of non-self-quenching counters. In addition to the counter voltage, the gain setting, bandwidth, and minimum pulse height setting for satisfactory operation were determined.

The factors governing the efficiency of the neutron counter have already been discussed. With the exception of control on the capture cross section by choice of moderator thickness, the other variables upon which the efficiency depends were fixed by the choice of counter design and gas pressure. Hence, no further investigation of this characteristic was warranted at this time.

Self-quenching counters suffer from the disadvantage that the quenching constituent is decomposed in the act of quenching. For this reason, the counter characteristics will vary with use. The pressure in the counter will increase and the plateau will become less flat. Concomitant with a pressure change, there will be an increase in the starting and operating potentials. A "life" of the order of 10^{10} counts is to be expected, however; so with tests employing low intensity sources, with precaution against operation at high over-voltages, and with limited use, a single counter served adequately for the present investigation. It should further be said that time appeared to have no effect upon the operating characteristics insofar as the counter had been carefully prepared, outgassed, and sealed.

C. Preparation of Radioactive Sodium

In the preparation of radio-sodium by cyclotron bombardment through the reaction

$$Na^{23} (d, p) Na^{24}$$

metallic sodium fails to produce high specific activity due to deterioration of the target material during bombardment. This fact has led to the recent development and use of metaborate compounds for internal cyclotron targets[47]. By virtue of the strong bond which forms between the fused metaborate compound and the supporting copper plate, good heat transfer is assured thereby providing maximum specific activity.

The target material is kept as thin as is compatible with efficient utilization of the beam. In the case of sodium metaborate, $NaBO_2$, the deuteron range may be calculated and an optimum thickness of target material (T) may be evaluated by the relation

$$T = 1.26 \times 10^{-4} \frac{M\left(E_i^{1.6} - E_j^{1.6}\right)}{\sum_i Z_i \Big/ (Z_i + 10)^{\frac{1}{2}}} \quad gm/cm^2$$

where M = molecular weight of sodium metaborate

E_i = deuteron energy, Mev (taken as 7 Mev here)

E_j = classical threshold energy for (Na + d) reaction

Z_i = atomic number of atom (i) in compound

This equation shows that for a circular target 1.7 cm in diameter, approximately 40 mg of target material are required for best results.

In the preparation of the target for bombardment, the following design and procedure has been found satisfactory. The target supports were constructed of 1.7 cm diameter, 3 inch length, copper stock. The target end was machined so as to

present an angle of 14° to the incident deuteron beam. This circular end face was then grooved with 50 lines per inch in a direction parallel to the plane of the beam. The sides of the grooves formed an angle of 45° to the face. This structure permitted more uniform cooling of the target material when deposited in a layer thin enough so as not to overflow the grooves. The opposite end of this support was next drilled out so as to form a hollow cylindrical cup of ½ inch inside diameter. After deposition of the metaborate upon the grooved face in the manner described below, this target head was silver soldered to the ¼ inch copper water cooling lines of the probe. The input water line was centered within the target cup and made to extend into the cup to within approximately 1/8 inch distance from the inner face of the target, while the outlet water line terminated at the end of the cup. By this design, the cooling water was made to enter the cup directly behind and centered on the target face, then sweep backward along the length of the copper cup to the outlet line. A water cooling flow rate of 90 cc/sec proved sufficient to remove the beam energy dissipated in the target. The temperature rise of the cooling water varied between 5° to 8° depending upon the deuteron beam current used.

The sodium metaborate can be obtained commercially under the trade name of "Kodalk." To prepare this for use as a target material, the crystals of $NaBO_2 \cdot 4H_2O$ were placed in a size 0 porcelain crucible and heated in an electric oven for two

hours at 100°C or until complete removal of the water of crystallization was assured.

The temperature of the oven was then raised to the melting point of $NaBO_2$ (966°C) and held until the compound fused into a homogeneous glassy melt. In this form the crystals are somewhat hygroscopic but may be safely stored until needed by placing the crucible under a bell jar containing some drying agent such as calcium chloride.

In the preparation of the sodium target, a small piece of the metaborate crystal weighing approximately 40 mg was placed on the grooved face of the copper cup. The latter was heated from the side with an oxy-gas torch while a reducing flame was played from above onto the target face. As soon as the metaborate began to melt, the reducing flame was removed for an instant and then reapplied. This procedure was necessary to permit the slight formation of a copper oxide layer on the target face without which the melted metaborate would not spread and wet the copper surface. In view of the fact that, if excessive amounts of copper oxide are allowed to form, the oxide floats up into the body of the metaborate, the advantages of limiting its formation to a minimum is apparent. To insure uniform distribution of the metaborate over the target support, the molten metaborate was spread smoothly over the surface of the copper with the aid of a tungsten wire. The oxy-gas flame was then removed and the reducing flame continued until the copper cooled to a temperature at which oxide formation was slight.

Upon cooling, the metaborate fuses into a crystalline mass which is uniformly distributed over the surface of the target plate and is tightly bonded to the copper backing. Any copper oxide formed on the metaborate surface is removed by gently brushing the surface with fine steel wool.

Because of the hygroscopic nature of $NaBO_2$, exposure of the target to the atmosphere is kept at a minimum and each target is prepared immediately before needed.

When the optimum target thickness is not exceeded, $NaBO_2$ exhibits very little vaporization or high temperature decomposition in a vacuum of 10^{-5} mm of Hg and can dissipate up to 20 kw/cm^2 through a water-cooled probe. Targets have been subjected to deuteron beam currents of 350 microamperes at 7 Mev for six to eight hours and show minimum deterioration.

To evaluate the efficiency[48] of a desired reaction when the element required for its production appears in compound form, we consider the stopping power, S, for positive ions of an element of atomic number Z. To a good approximation this is given by

$$S = kZ/(Z + 10)^{\frac{1}{2}}$$

In general, the stopping power of substances is additive. Hence the ratio of the number, N_{NaBO_2}, of molecules of $NaBO_2$ traversed by a projectile of given energy to the number of molecules, N_{Na}, of Na is

$$\frac{N_{NaBO_2}}{N_{Na}} = \frac{Z_{Na}/(Z_{Na}+10)^{\frac{1}{2}}}{\sum_{NaBO_2}\left\{Z_i/(Z_i+10)^{\frac{1}{2}}\right\}}$$

If ν_{Na} is the number of atoms of Na in a molecule of Na, and ν_{NaBO_2} is the number of atoms of Na in a molecule of $NaBO_2$, then the relative efficiency of $NaBO_2$ to Na for the nuclear reaction under consideration is (see reference 48)

$$\text{Rel.Eff.} = \frac{\nu_{NaBO_2} Z_{Na}/(Z_{Na}+10)^{\frac{1}{2}}}{\nu_{Na}\sum_{NaBO_2}\left\{Z_i/(Z_i+10)^{\frac{1}{2}}\right\}} = .32$$

Comparison of this result with the relative efficiency of other sodium compounds for this same nuclear reaction shows that higher yields than 32% are theoretically possible. However, from the standpoint of bonding strength, heat conductivity, melting point, energy dissipation, and convenience in handling, sodium metaborate ranks a favorite for use as an internal cyclotron target for the sodium reaction. This fact is substantiated by the work of Zachariasen[49] and Tazaki[50] who have shown that the meta-anions have the advantage of tending to form complex or network crystals. This suggests a possible reason why the metaborate compounds bond so effectively to copper.

The calculated yields for sodium targets prepared for use in the present investigation are based on published estimates

that an average yield of 25 mc of Na^{24} is obtained from 100 microampere-hours of 7 Mev deuteron bombardment of a $NaBO_2$ target[47].

D. Experimental Set-Up

In this investigation the neutron detector consisted of a BF_3 proportional counter surrounded by a paraffin form which acted as a moderator for slowing down the fast neutrons produced in the photo-disintegration process. A cadmium covering of 10 mil thickness completely surrounded the detector. This detector, as viewed from the position of the heavy water, presented a circular area through which the incident photo-neutrons had to pass in order to be detected. Only those neutrons emitted by the heavy water and contained in an angular opening of 5° could be slowed down and detected in the paraffin. As shown in Figure 2, the diameter of the detector was such that its fixed distance from the heavy water was 177.6 cm to give the desired angular opening.

In order to gain a high intensity of photo-neutrons, a large volume of heavy water is desirable. However, three factors militate against such a choice, namely, the increase in the photo-neutron scattering by the heavy water the larger the water volume, the fact that a larger volume means a greater departure from a point source of neutrons, and, finally, the angular distribution of the gamma rays effective in producing photo-disintegration may be increased beyond a prescribed

tolerance. To avoid these objections and still permit the effective use of as much as 30 cc of D_2O at one time, a toroid or anchor ring of small diameter copper tubing (.08 cm wall thickness) was filled with heavy water and placed concentric with the axis of the apparatus. The toroid had a radius of 10 cm; the internal diameter of the copper tubing, and hence of the heavy water was slightly less than 8 mm. With this choice of geometry, it was possible to meet the above requirements satisfactorily. Scattering by the heavy water was thereby reduced to a value not detectable outside the probable error of the data (see Section C, Chapter V); the point source requirement considering the distances involved was essentially satisfied; and the angular opening of the gamma rays was maintained within a value of 8.4° or less. (see Table II, Chapter V)

The Na^{24} gamma ray sources used throughout the experiment were prepared by cyclotron bombardment of Na^{23} with 7 Mev deuterons. By using beam currents of 300 to 350 microamperes for six or eight hours bombardment time, sources of 350 to 450 millicuries in strength were obtained. Immediately upon removal from the cyclotron, the source was placed on the axis of the heavy water toroid. By positioning the source at specified distances from the plane of the toroid and concentric thereto, it was possible to vary the angle, γ, between the primary gamma rays and the observed photo-neutrons. Figure 5 serves to illustrate the arrangement of the principal components of the apparatus. It is apparent that this geometry is such as to

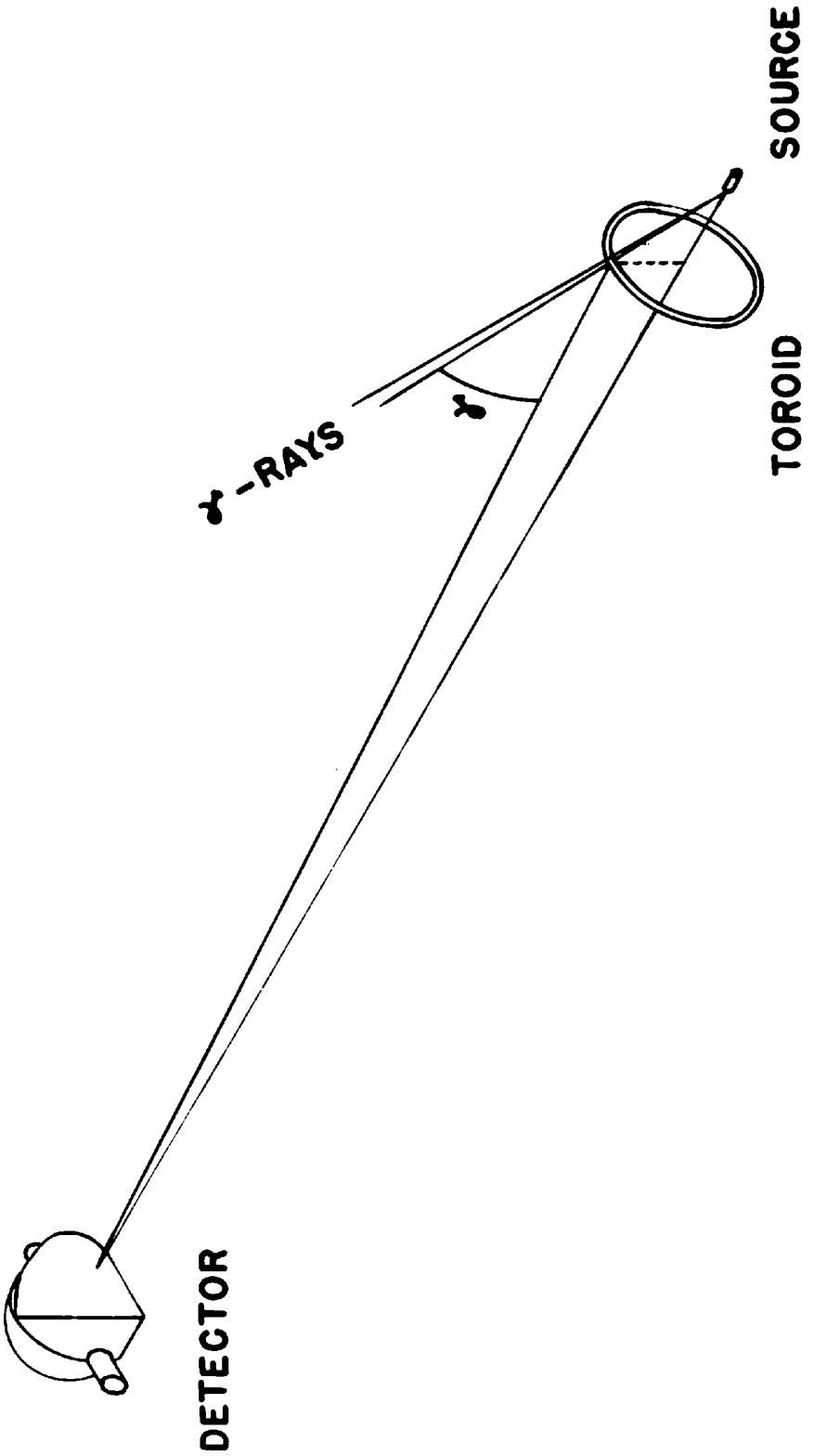

EXPERIMENTAL SET-UP
(NOT TO SCALE)

FIGURE 5

select for detection only those neutrons having the same direction (within the 5° angular opening) with respect to the primary gamma rays. As this direction is changed by movement of the sodium source, the gamma ray flux traversing the ring is likewise changed thereby necessitating a solid angle correction to the intensity. To keep this correction factor within a reasonably small range of values, the angle, γ, was varied from 90° to 45° in 15° steps. This required motion of the source throughout a total distance of 11 cm (see Table IV) as measured out along the axis of the toroid. For angles less than 45°, this distance increases rapidly with consequent decrease in neutron production. To avoid operating in a range where statistical fluctuation in the number of neutrons detected becomes appreciable, measurements at the smaller angles were avoided.

Using equation (15), it is possible then to determine the value of τ by measuring the number of neutrons projected at various angles with respect to the direction of propagation of the gamma rays. In principle, measurements at only two angles are sufficient.

The material forming the framework to support the components of the apparatus at fixed positions was kept as small as possible to avoid extraneous neutron scattering. Plates III and IV (Chapter V) are photographs of the complete apparatus showing the manner of suspension and support in the angular distribution tests outdoors. Plates I and II show the appara-

tus suspended from captive balloons. This arrangement was used in the inverse square law test to be described in the next chapter. In this test, a one-sixteenth inch diameter steel wire frame served to support the detector; this was fastened to linked sections of wire of the same dimension which in turn connected to the neutron source. For the angular distribution test (Plates III and IV), the steel wire frame extended from the heavy water toroid to the detector in order to provide good axial alignment of the several components. The housing supporting the gamma ray source was constructed of aluminum; this was fixed rigidly to the heavy water ring by a frame of one-sixteenth inch brass rod. This apparatus is shown suspended from the center of a 300 foot cable which extended between buildings.

In the scattering tests performed indoors and on the rooftop, the apparatus was supported 175 cm above the floor by ordinary laboratory tripods.

CHAPTER V

CONDUCT OF EXPERIMENT & SOURCES OF ERROR

A. Geometrical Considerations

Guided by the results of preliminary tests, it was possible to assign a specific set of geometrical conditions to the apparatus used in the measurement of the angular distribution of the neutrons. The requirement imposed upon the geometry demanded that, for the gamma ray source strengths available, the number of detected photo-neutrons be as large as possible while the angular openings of the neutron and gamma ray paths be maintained small. A 5° angular opening was selected for the neutrons while the gamma rays effective in producing photo-disintegration have a variable opening due to the finite size of the source and to the fact that the source distance varies with the angle, γ. The angular openings of the effective gamma rays corresponding to the several positions of the source are shown below in Table II

TABLE II

ANGULAR SPREAD OF GAMMA RAYS

ANGLE γ	90°	75°	60°	45°
ANGULAR OPENING	5.1°	7.2°	8.4°	7.8°

The effective diameter of the detector was set at 15½ centimeters. This dimension was prescribed in part by the experimentally determined optimum paraffin thickness of 5½ centimeters, mentioned earlier in Chapter IV, Section B, and by the diameter of the counter.

The toroids containing the heavy water were made of annealed copper tubing commercially available in standard sizes. Each toroid was formed by bending the tubing into a circle of ten centimeters radius and then silver soldering the adjoining ends. As a result of the test on scattering by the heavy water (see Section C below) only the toroid having an internal tube diameter of .795 centimeters was used in the angular distribution measurements. The measured volume of heavy water contained by this ring was 30.04 cc. As toroids of various internal tube diameters were used in the scattering tests, the data relating to these are given in Table III.

TABLE III

DIMENSIONAL DATA FOR HEAVY WATER TOROIDS
(10 cm radius)

Outside Diameter (inches)	1/8	1/4	5/16	3/8	1/2
Inside Diameter (cm)	.178	.439	.630	.795	1.092
Volume (cc)	1.56	9.53	18.87	30.04	59.27

With the above choice of geometrical conditions, the calculated detector range for a 5° opening is 177.61 centimeters, while the constant angle, χ, is 86° 46'. This is shown below in Figure 6.

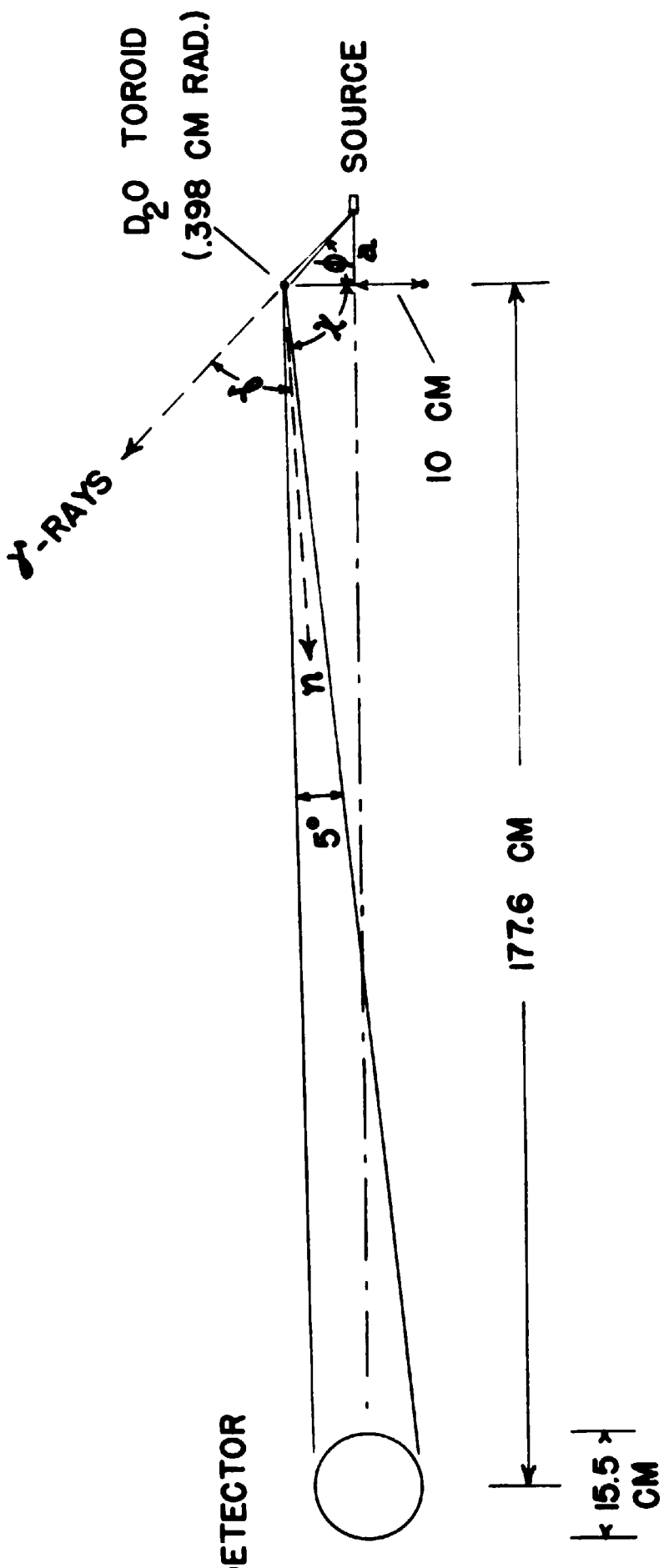

DIMENSIONAL VIEW OF APPARATUS
SCALE: 1 CM = 10 CM

FIGURE 6

The distance, a, and angle, ϕ, corresponding to various values of the distribution angle, γ', are shown in Table IV below.

TABLE IV

GEOMETRICAL DATA RELATING TO THE DISTRIBUTION ANGLE, γ'

ANGLE γ'	ANGLE ϕ	DISTANCE "a"
90°	3° 14'	.57 cm
75°	18° 14'	3.29 "
60°	33° 14'	6.55 "
45°	48° 14'	11.12 "

The relationship between these angles is $\gamma' + \phi + \chi = 180^{\circ}$.

The positioning of the gamma ray source in the suspension apparatus (see Plate III) was accomplished by machining stop grooves in the aluminum source support rod. A steel pin under spring pressure and mounted on the aluminum rod housing held the rod fast when it seated in one of the grooves. In this manner, the source distances, a, corresponding to the 90°, 75°, 60°, and 45° positions were quickly selected.

The precision of the geometrical arrangement was held to better than half a degree. For the tests indoors, the alignment was made optically; while in the outdoor suspension tests the equipment was weighted in such fashion as to prevent motion

of the detector relative to the toroid in excess of the above-mentioned precision. This alignment is more precise than the experimental error of the measurements necessitate.

B. Extrinsic Sources of Neutrons

In considering the sources of errors which may occur in a low intensity experiment of this type, it is reasonable to inquire into the possibility of neutron formation by reactions other than the H^2 (γ,n) reaction under investigation. If such neutron sources are present even at extremely low intensities, their contribution to the measured photoeffect would be difficult if not impossible to estimate and, of course, could materially influence the interpretation of the data.

Toward this end, we shall consider in turn the various possible neutron producing reactions which in principle are present. The question as to whether these reactions are energetically possible, and thus able to produce extrinsic sources of neutrons, remains to be answered here. It is sufficient to consider but three possible types of reactions, the (p, n), (n, 2n), and (γ, n) reactions, since no other nuclear processes are present which may result in the formation of neutrons. Further, the types of nuclei which are subjected to the photo-proton bombardment are limited to those composing the toroid and contained therein.

Cu^{63}(p, n)Zn^{63}: This reaction has been investigated by Strain[51] and by Delsasso et al[52]. The product nucleus is a

positron emitter with half-life of approximately 38 minutes. Data for a thick target excitation curve fixes the proton threshold energy at 3.6 Mev. With protons of maximum energy of .29 Mev available from the process of photo-disintegration, this reaction is excluded as a possible source of neutrons.

$Cu^{65}(p, n)Zn^{65}$: A long lived activity of 250 days half-life is observed in copper samples subjected to long bombardment[53]. This is explained by a transformation of Zn^{65} to Cu^{65} as a result of the capture by zinc of one of its K-electrons. Gamma rays are emitted by the copper and are only slightly internally converted. The absorption curve in lead shows the gamma rays to be reduced to half value by 9.6 grams per cm^2 of lead[54]. This indicates an energy of 1.0 Mev for the gamma rays. More recently Shoupp, Jennings, and Jones[55] have investigated the threshold for this (p, n) reaction and report a value of 2.16 Mev.

$O^{18}(p, n)F^{18}$: Only the oxygen isotope of atomic weight 18 undergoes a (p, n) reaction with the production of F^{18}; the remaining stable isotopes of oxygen undergo (p, γ) reactions only. Investigation [56] of the excitation function shows that the F^{18} activity sets in sharply at 2.6 Mev for both thick and thin targets.

$H^2(p, n)2H^1$: From statistical arguments one would expect the cross section for this three-particle disintegration to be

very low near threshold. Conservation of momentum requires that the incident proton energy at threshold be $(3/2)W_1$, where W_1 represents the binding energy of the deuteron. Hence, an energy of 3.3 Mev would be required. Smith and Richards[57] have made an experimental determination of the threshold and find agreement with this energy value.

$Z^A(n, 2n)Z^{A-1}$: We generalize this reaction for any nucleus of atomic number Z since all nuclei contained in the apparatus are exposed to the neutron radiation. It is clear that this reaction, having two neutrons as end products, requires at least an amount of energy corresponding to the binding energy of the neutron in the nucleus, i.e. about 8 Mev[58]. Hence, this reaction cannot possibly take place since the incident photo-protons possess only .29 Mev energy.

$Z^A(\gamma, n)Z^{A-1}$: On the basis of the statistical theory of nuclear reactions (evaporation model), the (γ, n) yields for the heavier nuclei depend quite sensitively on the binding energy of a neutron to the nucleus in question. Thresholds for elements of atomic number up to 47 have been measured by Baldwin and Koch[59] who find 10.9 Mev for the Cu^{63} reaction and 14.2 Mev for the Fe^{54} reaction. No reaction was reported having a threshold energy less than 9.3 Mev.

In consideration of the above cases of proton, neutron, and gamma ray processes which could give rise to neutrons as reaction products, we see that in each instance insufficient

energy is available for the process to proceed. With the exception of possible contaminant nuclei present in the toroids, the bulk of the material exposed to the photo-protons can experience no reactions involving the emission of neutrons.

The question of neutron formation by photo-disintegration of deuterons present in the isotopic ratio of 1 part in 5000 in the paraffin form surrounding the counter may be justifiably raised. Such an effect, while present to a slight degree, is on the average cancelled out. All neutron background determinations were made with no other change in the apparatus except the removal of the heavy water toroid - the paraffin form remaining in position about the counter throughout a complete experimental run.

C. Scattering by the Heavy Water

The problem of the scattering of photo-neutrons by the heavy water requires careful attention. So far as the isotropic component of the photoeffect is concerned, the scattering would have no influence upon the measured angular distribution. This is not the case, however, for the $\sin^2$ component. The net result would be to enhance the isotropic component at the expense of the anisotropic component. For this reason the effect of the scattering by the heavy water must be kept small.

An attempt was made to minimize this effect by the choice of the geometrical configuration assigned to the heavy water. In the interest of high neutron intensity, as large a volume

of water as possible is to be desired. However, in opposition to this choice, it is important to keep the length of water path through which the neutrons must travel as small as possible. Toward this end, it was apparent that both requirements could be met in part at least by forming the water into the shape of a toroid the radius of whose section would be kept as small as possible consistent with the neutron intensity desired. Having made this choice, it became necessary to investigate the optimum toroid dimensions which would allow substantial intensity without excessive scattering.

Into each of four toroids having outside diameters of 1/4, 5/16, 3/8, and 1/2 inches (see Table III), a constant volume (9.53 cc) of D_2O was added. This volume completely filled the 1/4 inch toroid. The remaining toroids were then filled to full capacity with H_2O such that the percentage of H_2O to D_2O was 0%, 98.2%, 215.5% and 522.6% respectively. These data are shown in Table V, columns 2, 3, and 4.

Using toroids filled in this manner, it was possible to investigate the effect of the increased volume of water upon the scattering while at the same time to hold constant the number of photo-neutrons produced in the photo-disintegration process. Any change in the number of neutrons detected could quite correctly be attributed to the effect of the additional water upon the scattering.

A Na^{24} gamma ray source was prepared by a six and one-half hour cyclotron bombardment at an average deuteron beam current

of 350 microamperes. Observations of one hour duration were made for each toroid. Two background observations each of one hour duration were made near the start and at the end of the run - an empty copper toroid replacing the water-filled toroids during these periods. This background amounted to an average value of 1.29 counts per minute. The resulting data for $\gamma = 90^{\circ}$ are shown tabulated in Table V. Because of the decay of the sodium source during the course of an experimental run, it is necessary to apply a decay correction factor (Table V, column 8) to the data so as to normalize the counting rates to a constant source intensity (see Section F, 1, below). For this purpose, a Cenco-Harrington timer consisting of a revolution counter driven by a synchronous motor was operated throughout the course of each experiment to record the "age" of the sodium source in seconds. The "Observation Period" listed in column 5 of Table V shows the initial and final readings of the timer, in seconds, for each test. The data for this test are shown plotted in Graph No. 5 in which the number of photo-neutron counts per minute is plotted against the percentage of H_2O to D_2O by volume.

The interpretation given to this result rests in general upon the fact that, within the probable error of the data, no increase in intensity is apparent for toroid volumes up to 30 cc (3/8 inch toroid) for which the radius of the toroid section is .398 cm. As the volume becomes greater, however, those neutrons which travel in the plane of the toroid have

TABLE V

DATA FROM D_2O SCATTERING TEST

1	2	3	4	5	6	7	8	9
TOROID	VOLUME (cc) D_2O	VOLUME (cc) H_2O	PERCENT H_2O to D_2O BY VOLUME	OBSERVATION PERIOD (sec)	TOTAL NO. COUNTS (with background)	TOTAL NO. COUNTS (without background)	DECAY FACTOR	NO. COUNTS (per min)
1/4	9.53	0.00	00.0	1750-5350	537	459.5	1.0225	7.83 $\pm$.28
BACKGRD	--	--	--	5430-9030	85	--	--	--
5/16	9.53	9.35	98.2	9125-12725	474	396.5	1.1260	7.44 $\pm$.30
3/8	9.53	20.52	215.5	12835-16435	459	381.5	1.1820	7.52 $\pm$.31
1/2	9.53	49.75	522.6	16540-20140	519	441.5	1.2400	9.13 $\pm$.34
BACKGRD	--	--	--	20320-23920	70	--	--	--

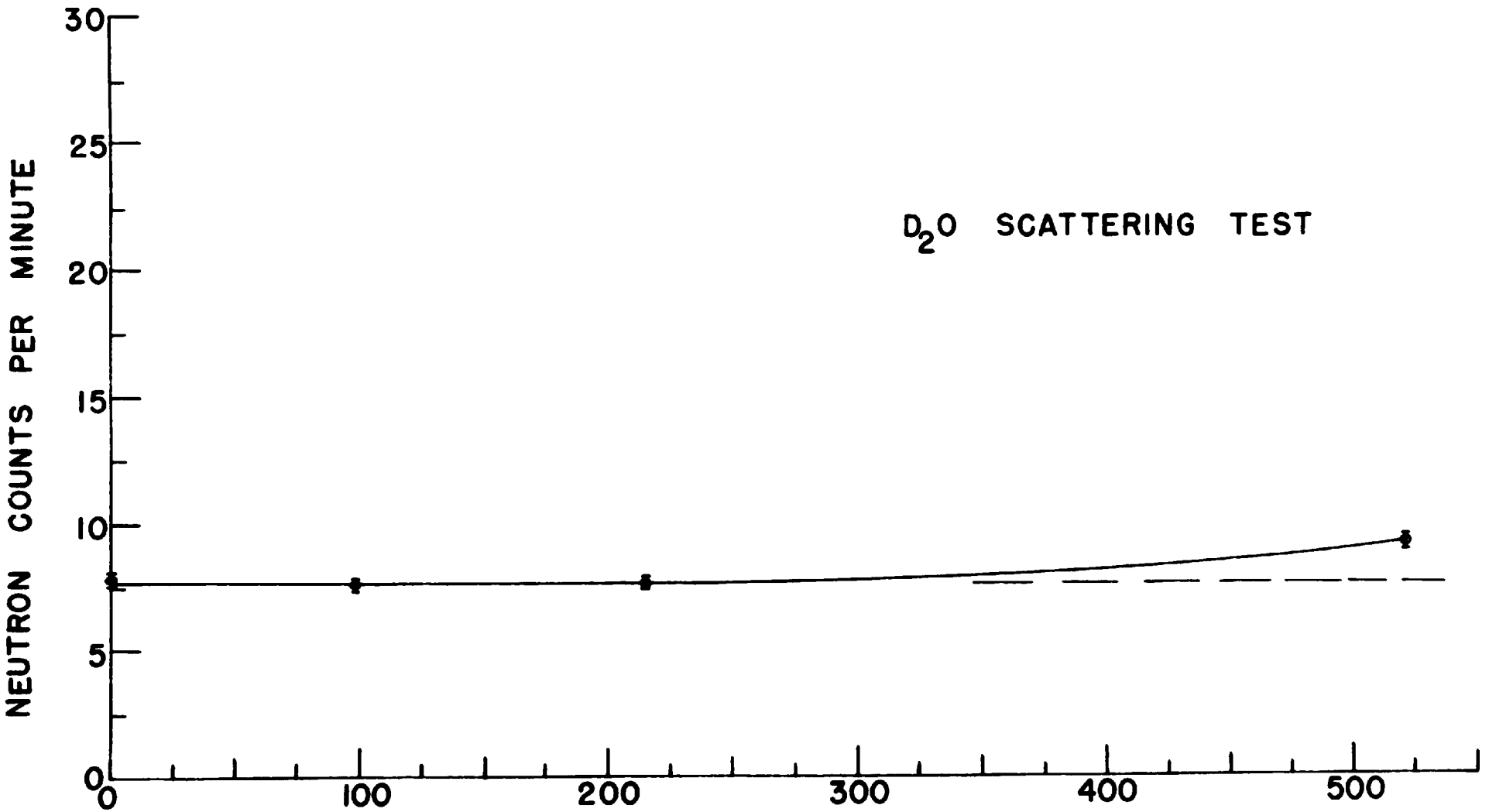
D_2O SCATTERING TEST
NEUTRON COUNTS PER MINUTE
30
25
20
15
10
5
0
0
100
200
300
400
500
PERCENTAGE H_2O TO D_2O BY VOLUME

GRAPH NO. 5

greater probability for scattering since their path lengths in water have become greater. Hence, some neutrons which were not initially directed toward the detector may now suffer single or multiple scattering and be recorded. These scattered neutrons augment the unscattered intensity recorded for the smaller volumes. Thus, a rise in the curve sets in at volumes for which the amount of scattering is detectable outside the probable error of the counting rate. In consequence of this fact, the 3/8 inch toroid was used throughout all subsequent angular distribution tests. This choice permitted as large a neutron intensity as possible consistent with a minimum detectable scattering effect.

D. Scattering by the Walls

A potential source of error in any experiment in which fast neutrons are formed at one position and detected as slow neutrons at another position removed from the source is that due to the scattering of the neutrons by parts of the apparatus and by the walls of the room. As mentioned in Chapter IV, Section D, the material forming the framework of the apparatus, and the supports for holding the components of the apparatus at fixed positions were kept sufficiently thin to make their contribution to this effect negligible. However the contribution from the walls of the room is difficult to estimate. For this reason, it was necessary to measure the scattered neutron intensity to determine the extent to which this effect influenced the experiment.

The scattering by the walls of the room was studied by measuring the deviations from the $1/r^2$ law for the neutrons observed with the detector at various distances from a small photo-neutron source. For this purpose a freshly bombarded Na^{24} source was surrounded by a metal cup containing 190 cc of heavy water. This and the detector heretofore described were mounted six feet above the floor of a medium sized laboratory room whose dimensions in meters was 7 x 14 x 4. Readings of the neutron intensity were made with the photo-neutron source placed at various distances from the detector. The latter was maintained at a fixed position in the center of the room.

The results of this test, corrected for decay of the source and with background (approximately one count/min.) subtracted, are given in the column marked "Indoors" of Table VI. The first column gives the source-detector distance in meters.

Plotting observed photo-neutron intensity per minute versus distance in meters on a logarithmic scale, the upper curve of Graph No. 6 shows the result. It is apparent that the deviation from the inverse square law is extremely large; the exponent evaluated for these data was found to be -1.15 instead of -2.

In consequence of this result, the apparatus was next mounted on the parapet fringing the roof of a 4-story laboratory building. The detector, still supported on a thin stand

six feet high, was placed at one corner of the parapet. Its overall height above the roof was 8½ feet. The neutron source, consisting of 150 cc of heavy water surrounding a Na^{24} target of approximately 400 mc strength, was similarly mounted on top of the parapet. By moving the source at various intervals along one side of the building, the variation of intensity at the detector could be recorded.

The data resulting from this test, when corrected for decay and with background (approximately three counts/min.) subtracted, are shown in the column marked "Roof-top" of Table VI.

A logarithmic plot of these data, normalized at the one meter position with the previous data taken indoors, is shown on Graph No. 6. A considerable improvement toward an inverse square fall-off is apparent, the exponent now decreasing to -1.66.

To reduce still further the effect of neutron scattering by the surrounding objects, the equipment was adapted so as to permit measurements aloft. Ten Dewey and Almy (Darex N-4) neoprene captive balloons were each inflated to approximately six feet diameter with hydrogen to give a lifting force of three and one-half pounds per balloon. The equipment, consisting of cadmium-covered paraffin moderator, counter, preamplifier, filter box, and wire basket, weighed approximately twelve pounds; the heavy water cup and source weighed approximately one pound; the rubber-covered, five conductor, shielded cable and the rubber-covered, unshielded, high voltage cable

which supplied power to the preamplifier and counter weighed approximately fourteen pounds. The ten balloons were linked together into a compact group so as to minimize excessive jarring of the apparatus which otherwise would occur if the balloons were allowed to separate and then be blown against each other. The distance between source and detector was made variable in intervals of one meter by linking together a number of one-meter sections of 1/16 inch stranded steel cable with snap hooks. By lowering the apparatus, sections of cable could be added or removed as desired. The mooring line consisted of nylon rope having a 150 pound breaking strength. This line was controlled by hand-operation of a windlass.

Plate I is a vertical view showing the manner in which the apparatus was suspended from the mooring line. The weight of the power cables was removed from the detector by looping these cables back to the line as shown.

Plate II is a photograph of the side view of the apparatus in flight. The captive balloons were positioned approximately one hundred and twenty-five feet above the apparatus so as to minimize the effect of scattering by the hydrogen gas. During the course of a run, the apparatus was maintained at an average distance of 60 feet from the building.

Using 190 cc of D_2O, intensity measurements were taken at six positions in random order. The data corrected for decay of the source and for background (approximately three counts/min.) are shown in the column marked "Aloft" of Table VI.

TABLE VI

DATA FROM INVERSE SQUARE LAW TESTS

DISTANCE (meters)	NO. COUNTS PER MINUTE		
	Indoors	Roof-top	Aloft
1	2049	957	2115
2	868	294	529
3	556	154	228
4	399	90	126
5	308	65	82
6	243	47	58
7	220	38	--

A logarithmic plot of these data, normalized at the one meter position with the previous data, is shown on Graph No. 6. The dashed line is that corresponding to an inverse square fall-off.

The consistency of the data in obeying the inverse square law when the apparatus is kept clear of walls is apparent. To make unambiguous tests on the angular distribution of the photo-neutrons arising from the photo-disintegration of the deuteron, these results have shown that the apparatus must be suspended outdoors and at least 60 feet away from surrounding objects. Such a procedure effectively eliminates the need for a wall scattering correction to the data. The urgency of this requirement is emphasized by the above tests and by the fact

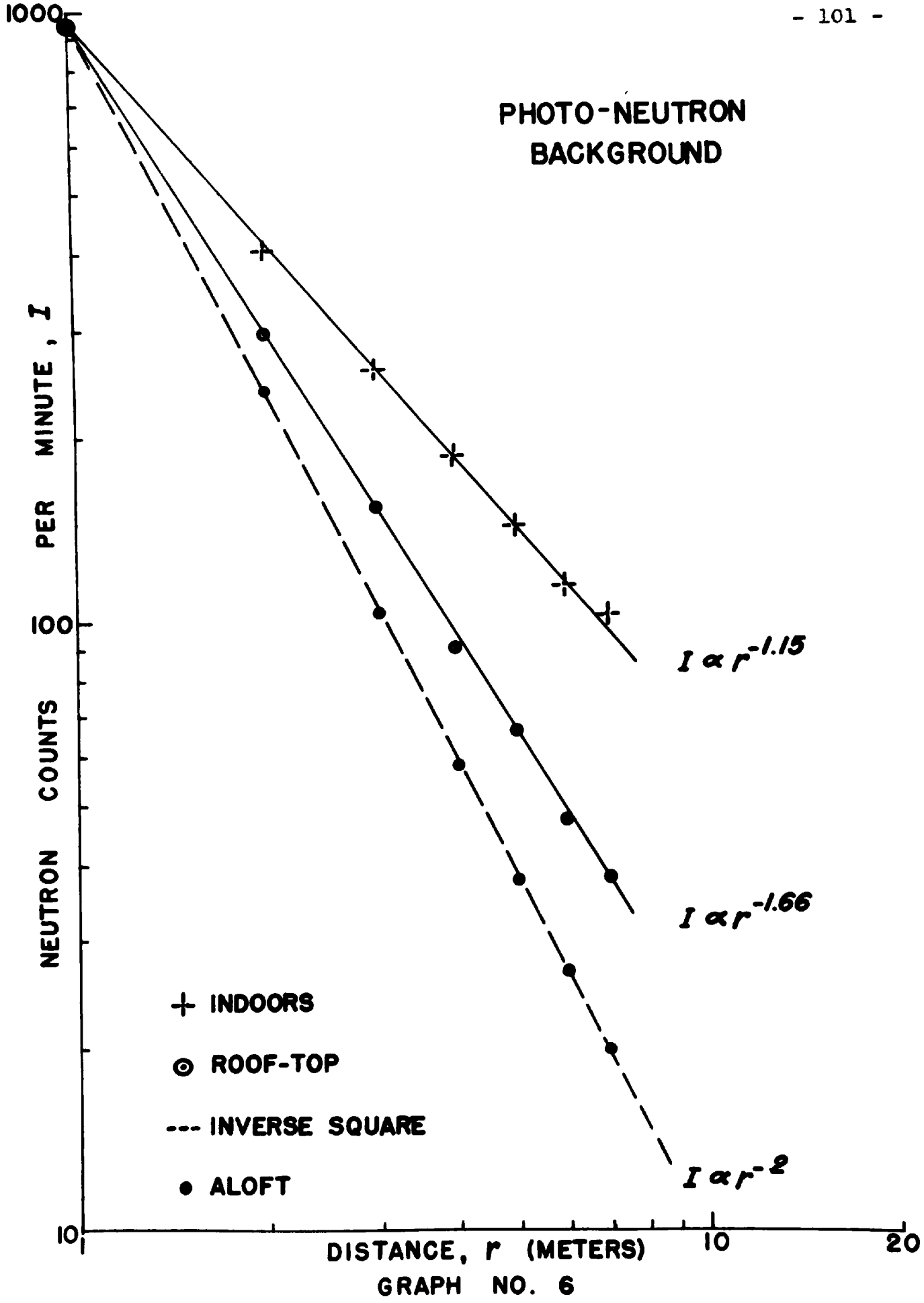
PHOTO-NEUTRON
BACKGROUND
1000
100
10
NEUTRON COUNTS PER MINUTE, I
$I \propto r^{-1.15}$
$I \propto r^{-1.66}$
$I \propto r^{-2}$
+ INDOORS
⊙ ROOF-TOP
--- INVERSE SQUARE
● ALOFT
10
DISTANCE, r (METERS)
20

GRAPH NO. 6

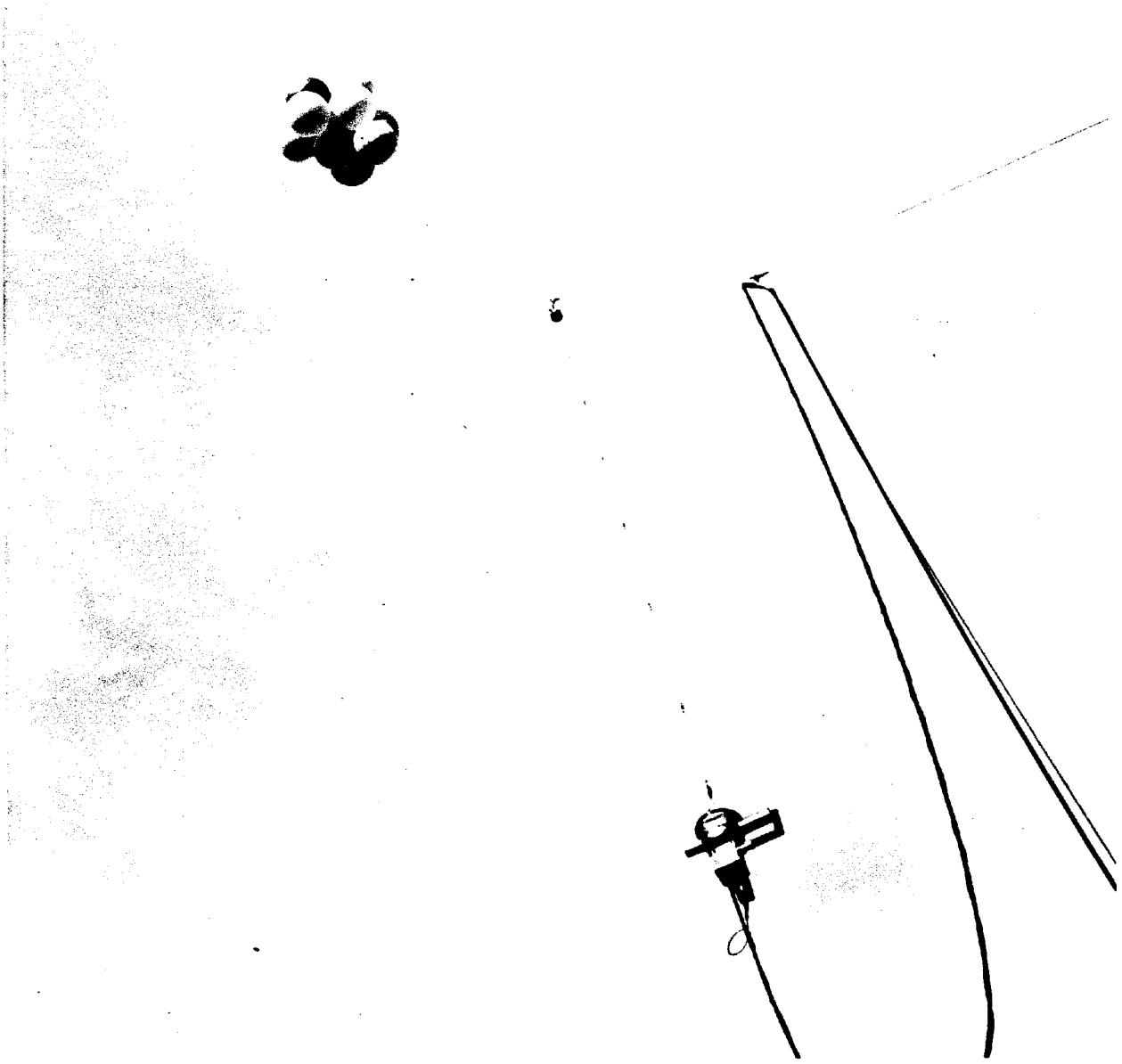

PLATE I

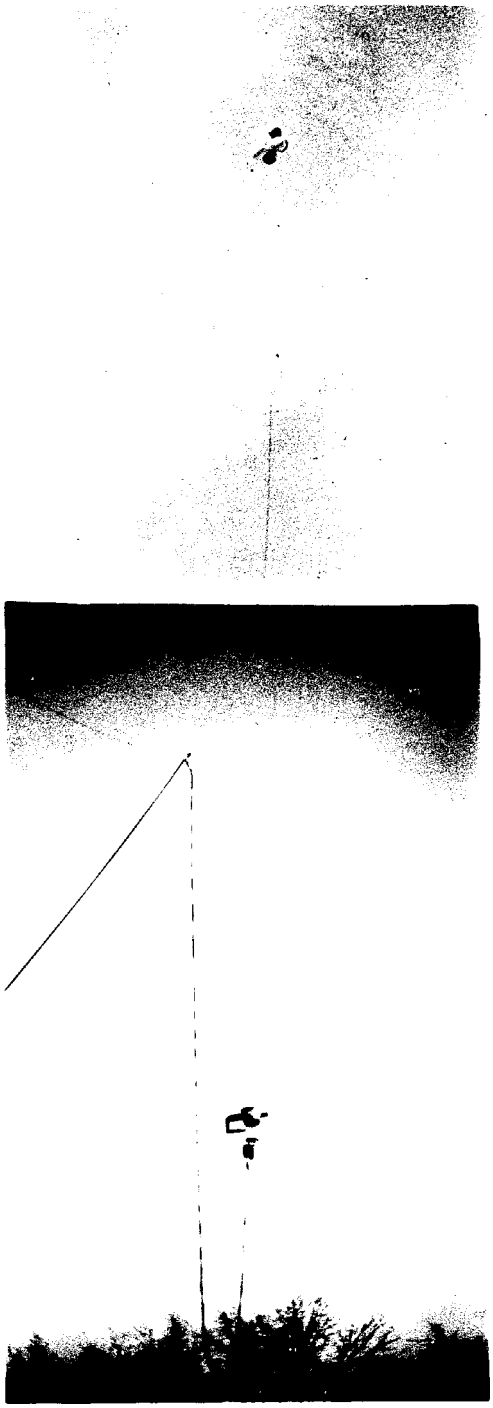

PLATE II

that the magnitude of the scattering correction for an indoor test would be difficult if not impossible to estimate correctly.

E. Measurements Using Out-of-Door Suspension

The conduct of the experiments on the angular distribution measurements was altered to permit an out-of-doors test without the use of balloons. For this purpose a three hundred foot suspension cable (1/8 inch stranded steel) was fastened so as to extend between structures atop the roofs of two 4-story buildings. The cable cleared the roofs of these buildings by a distance of approximately 15 feet. The clearance between buildings was 200 feet. The apparatus previously described at the end of Chapter IV and shown in Plates III and IV was equipped with nylon lines to permit its being drawn out with the aid of pulleys to a point midway between and slightly above the two buildings. In this fashion the equipment remained suspended 100 feet from the buildings and approximately 90 feet above the ground. Checks on the inverse square law in the manner described above showed that with this arrangement the scattering effect was absent when the apparatus occupied the operating position at the center of the cable. As example, the results of one such test gave hourly counts, less background, of 1980, 121, and 42 at the 1, 4, and 7 meter positions, respectively.

In the conduct of the angular distribution measurements, the activated source of sodium, mounted on its support rod,

was placed in the aluminum holder shown above the toroid in the upper frame of Plate III. An empty or heavy-water filled toroid shown clamped to the wire basket allowed either a background or an angular distribution measurement. The detector, with accompanying preamplifier and filter box, was supported by the four stranded cables which extended down from the toroid as shown in the lower frame of Plate III. These cables in turn fastened to an empty copper toroid which encircled the top portion of the cadmium-covered paraffin form. This toroid served to prevent the cables from cutting into the paraffin. Only the sensitive volume of the counter was enclosed in the paraffin form. The horizontal portions seen extending beyond the form on either side consisted of the shielding cup and sleeve and were not regions sensitive to neutron detection. However, these portions were covered with cadmium sheet to permit absorption of slow neutrons which approached the sensitive volume from either end of the counter.

Between operations, the apparatus was drawn in, the source reoriented to a new position by means of the stop grooves in the source support rod, and then the apparatus was drawn out to its operating position at the center of the suspension cable.

A total of six complete and independent measurements were made of the angular distribution at the 45°, 60°, 75°, and 90° positions. Observation at each position lasted for one hour. Without exception, the runs were made at night and during the early morning hours when interference from other apparatus was at a minimum. The results of the six tests are shown in Table VII.

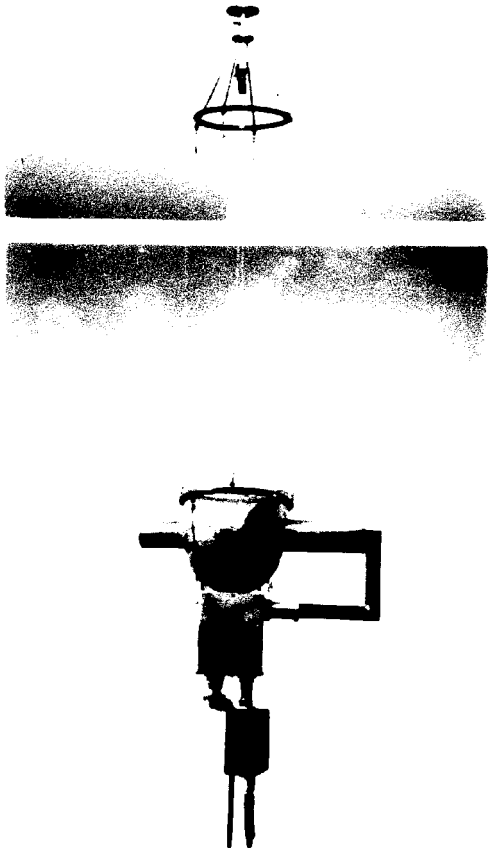

PLATE III

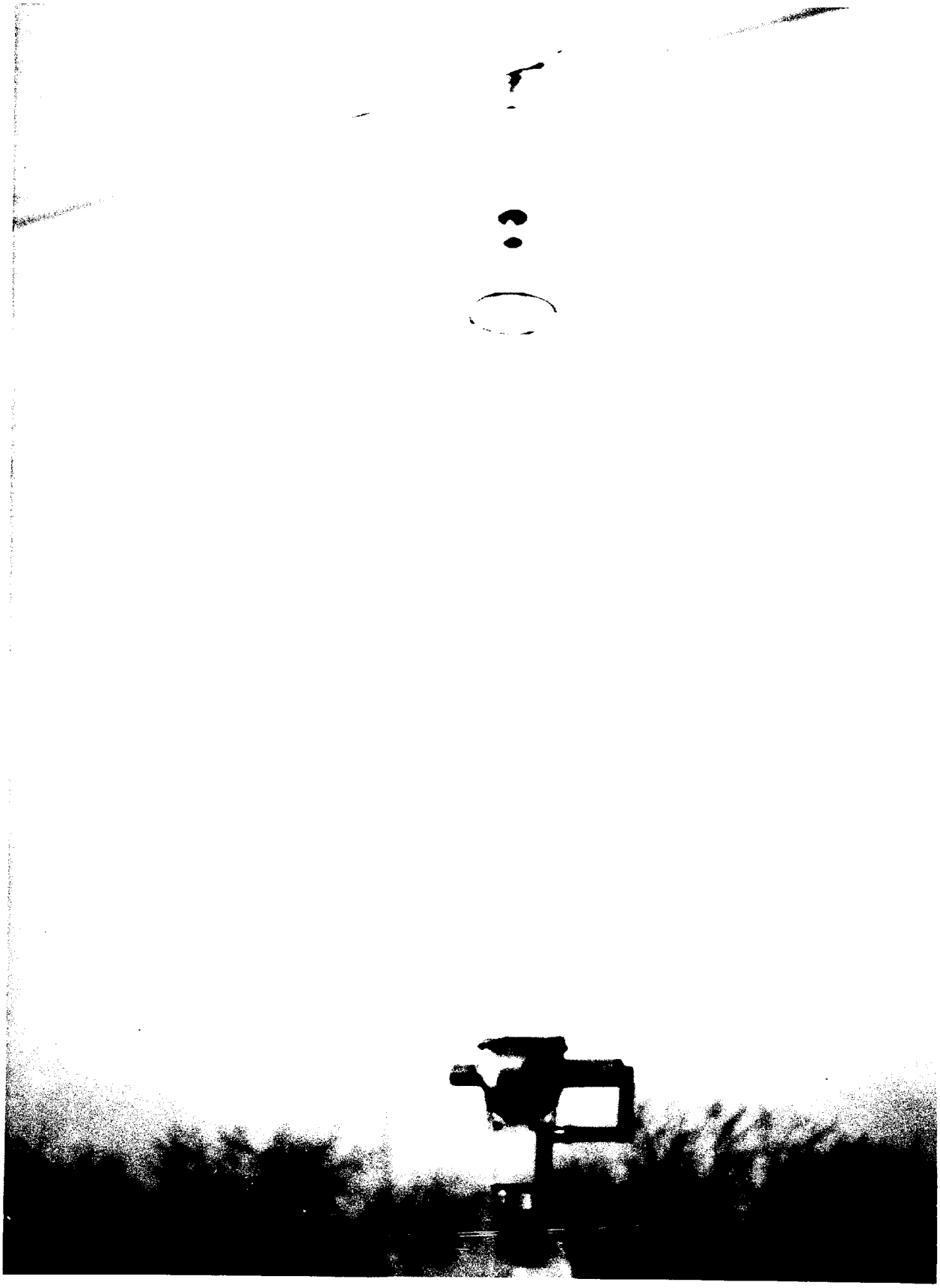

PLATE IV

TABLE VII

DATA FROM ANGULAR DISTRIBUTION MEASUREMENTS

Toroid: 3/8 inch
Pulse Height Setting: 80
Counter Voltage: 2100 volts

	POSITION	OBSERVATION PERIOD (seconds)	TOTAL NO.CTS/hr (with background)	NO.COUNTS/min (less background)
TEST #1	BACKGROUND (45°)	7640 - 11240	112	--
	45°	12030 - 15630	476	6.067
	60°	16015 - 19615	841	12.150
	75°	20045 - 23645	1171	17.650
	90°	23930 - 27230	1292	19.667
	BACKGROUND (90°)	28000 - 31600	112	--
TEST #2	BACKGROUND (45°)	0000 - 3600	103	--
	45°	4376 - 7976	392	4.800
	60°	8269 - 11869	686	9.700
	75°	12233 - 15833	943	13.983
	90°	16118 - 19718	1042	15.633
	BACKGROUND (90°)	10125 - 13725	105	--

TABLE VII (cont'd)

DATA FROM ANGULAR DISTRIBUTION MEASUREMENTS

	POSITION	OBSERVATION PERIOD (seconds)	TOTAL NO.CTS/hr (with background)	NO.COUNTS/min (less background)
TEST #3	BACKGROUND (90°)	8900 - 12500	91	--
	90°	13108 - 16708	676	9.767
	75°	17070 - 20670	566	7.933
	60°	21110 - 24710	386	4.967
	45°	25100 - 28700	221	2.183
	BACKGROUND (45°)	29440 - 33340	89	--
TEST #4	BACKGROUND (90°)	2900 - 6500	108	--
	90°	6880 - 10480	860	12.567
	75°	10730 - 14330	721	10.250
	60°	14600 - 18200	484	6.300
	45°	18530 - 22130	276	2.833
	BACKGROUND (45°)	22500 - 26100	104	--

TABLE VII (cont'd)

DATA FROM ANGULAR DISTRIBUTION MEASUREMENTS

	POSITION	OBSERVATION PERIOD (seconds)	TOTAL NO.CTS/hr (with background)	NO.COUNTS/min. (less background)
TEST #5	BACKGROUND (45°)	6100 - 9700	112	--
	45°	10150 - 13750	381	4.508
	90°	14056 - 17656	1095	16.408
	60°	17898 - 21498	630	8.658
	75°	21764 - 25364	867	12.608
	BACKGROUND (90°)	25740 - 29340	109	--
TEST #6	BACKGROUND (45°)	0000 - 3600	116	--
	60°	3910 - 7510	541	7.067
	45°	7780 - 11280	308	3.183
	90°	11670 - 15270	807	11.500
	75°	15625 - 19225	678	9.350
	BACKGROUND (90°)	19610 - 23210	118	--

F. Treatment of the Data

The neutron intensity recorded at each angular position and shown in Table VII requires several corrections before useful information may be obtained from the data. One such correction concerns the decay of the radio-sodium; a second correction must be applied to the recorded intensity by virtue of the fact that the gamma ray flux streaming through the heavy water toroid varies with the axial distance "a". We consider each of these corrections separately in the following sections.

1. Decay Correction

During the course of an experimental observation, the radio-sodium source of initial intensity, N_o at time, t_o, continuously decays with a half-life, T, of 14.8 hours. In order to express the observed neutron intensity for all angles in terms of a constant gamma ray intensity, an observation made at time t_2, after the initial starting time t_1, must be corrected by a factor N_1/N_2, where N_1 and N_2 are the source strengths at time t_1 and t_2, respectively. Consequently, we have by the law of radioactive decay, $N_1 = N_o e^{-\lambda t_1}$, that

$$\frac{N_1}{N_2} = \frac{N_o e^{-\lambda t_1}}{N_o e^{-\lambda t_2}} = e^{\lambda(t_2 - t_1)}$$

The decay constant, λ, is related to the half-life expressed in seconds by the relation $\lambda = \frac{0.6932}{T}$. Hence, for T = 14.8 hours and $(t_2 - t_1)$ expressed in hours, we have:

$$\frac{N_1}{N_2} = e^{.04685(t_2 - t_1)}$$

To indicate the order of magnitude of this decay correction for radio-sodium for hourly observation periods (t_k) up to ten hours after the initial starting time, t_1, the following table is prepared.

$t_k - t_1$	N_1/N_2
0	1.000
1	1.048
2	1.098
3	1.151
4	1.206
5	1.264
6	1.325
7	1.388
8	1.455
9	1.524
10	1.598

In the application of this correction to the data of the previous section, an average decay correction over a one hour period was applied to the number of counts recorded for that period. The beginning (t_1) and final (t_k) observation times for a single hourly observation were expressed in seconds after the initial time, t_1, in the computation of the actual decay correction to be applied to the data.

2. Solid Angle Correction

The gamma ray flux density at the toroid is a function of position of the sodium source. This source is moved along the

toroid axis in order to vary the γ-angle, between the neutron direction and gamma ray direction, to the preselected values of 45°, 60°, 75°, and 90°. The correction to be applied may be evaluated on consideration of the dependency on "a" of the solid angle subtended by the toroid at the source position - the toroid defines an annular hollow cone with center at the source. However, this more complicated procedure leads to the same result as that found by application of the inverse square law. Expressing the gamma ray intensity, or solid angle, at the toroid as a function of "a" we have simply

$$\Omega \propto \frac{1}{a^2 + r^2}$$

where r, the radius of the toroid, has a value of 10 cm. (see Figure 6)

In the application of this correction, we need only consider the ratio of intensities, or of solid angles, for any two positions of the source. In this case, we see that the correction factor is independent of the radius of the toroidal section. If we normalize this correction to the 90° position (a = .57 cm), we have the following correction factors which are to be applied to the neutron intensities recorded at the several positions:

TABLE VIII

SOLID ANGLE CORRECTION FACTORS

γ-ANGLE	DISTANCE, a (cm)	CORRECTION $\frac{\Omega_{90^\circ}}{\Omega_i}$
90°	.57	1.0000
75°	3.29	1.1046
60°	6.55	1.4244
45°	11.12	2.2293

3. Calculation of Probable Error

From the analysis of the statistics of random distributions which apply when the events to be counted are independent of each other, it has been shown[60] that the standard deviation, D_1, to be expected of the observed number of counts from the true average is given as simply

$$D_1 = \sqrt{N_1}$$

where N_1 is the total number of counts observed. The probable error is then defined as $0.6745\ D_1$.

In the present investigation, it is necessary to distinguish the background counting rate from the total counting rate by separate experiments and then to calculate their difference to give the true counting rate. Hence, if the standard deviations

of these two sets of data are D_1 and D_2, the deviation, D, of the difference will be just the square root of the sum of the squares of D_1 and D_2. Consequently, if N_1 counts are produced by the photo-neutrons plus the background and N_2 by the background alone, then the standard deviation for the photo-neutron count alone will be

$$D = (N_1 \pm N_2)^{\frac{1}{2}}$$

In Chapter VI, it will be shown that, to evaluate the ratio of the photomagnetic to the photoelectric cross sections, it is necessary to propagate the standard deviations, or probable errors, of independent sets of data through the operations of multiplication and division. By employing the standard results of error theory, e.g. equation 102, page 165, L. D. Weld's "Theory of Errors and Least Squares", MacMillan Company (1916), to these operations, we find in each case that propagation of the deviation to the product or quotient is properly performed by taking the square root of the sum of the squares of the relative or percentage deviations.

The above procedures have been employed in evaluating (see Table XII) and propagating (see Table XIV) the probable error of the data which is presented in Table XI, Chapter VI.

As will become apparent in the next chapter, the treatment of the data has the consequence of producing some results which are more reliable than others. It is customary in such cases to assign weights to the series of experimental values. Assuming

a law of normal frequency distribution, it has been shown that, for unequally weighted mean values, the weights w_1, w_2, w_3, ... w_n are to be taken inversely proportional to the square of the probable errors p_1, p_2, p_3, ... p_n associated with those values. Having made this assignment, we are faced with the problem of combining several unequally weighted intermediate mean values of a quantity into a grand mean and its probable error. This problem has been amply treated by Worthing and Geffner[61]. We shall follow the results of these authors in the subsequent treatment of the problem.

We consider a set of intermediate means, $\bar{X}_1$, $\bar{X}_2$, $\bar{X}_3$, ... $\bar{X}_n$, corresponding to the several mean values of the experimental data. Let $p_{\bar{X}_1}$, $p_{\bar{X}_2}$, $p_{\bar{X}_3}$, ... $p_{\bar{X}_n}$ be their probable errors, respectively. Then, (see equations 27 and 28, Chapter VIII of reference 61) the set of intermediate means with known probable errors may be combined into a grand mean, $\bar{\bar{X}}$, and its probable error by the equations

$$\bar{\bar{X}} = \frac{\sum \left(\bar{X} \frac{1}{p_{\bar{X}}^2}\right)}{\sum \frac{1}{p_{\bar{X}}^2}} \qquad (18)$$

$$p_{\bar{\bar{X}}} = \frac{1}{\sqrt{\sum \frac{1}{p_{\bar{X}}^2}}} \qquad (19)$$

Equations (18) and (19) may be applied to a set of intermediate means when no constant errors have entered into some or

possibly all of the determinations, i.e. when the intermediate means are consistent. To justify use of these equations, it is necessary to subject the intermediate means to a test for consistency. For this purpose the Rossini and Deming test may be used (see reference 61, page 198). Thus, two means may be considered consistent when they do not differ by more than twice the sum of their standard deviations. As the experimental data in this investigation have been subjected to the above test and found to be consistent, equations (18) and (19) have been used in the treatment of the data.

CHAPTER VI

RESULTS AND CONCLUSIONS

A. Experimental Results

From the results of the theoretical analysis of the nuclear photoeffect as outlined in Chapter II, we have seen that the total cross section consists of an isotropic component due to magnetic interaction and an anisotropic component due to electric interaction. The differential cross section of the latter has, by equation (5), been shown to conform to a $\sin^2$ distribution. In consequence, we may assume that, at the angle, γ', between the direction of the incident gamma ray and the ejected photo-neutron, the average intensity of the photo-neutrons can be described by a relation of the form

$$\bar{I}(\gamma') = \frac{\int_{\gamma_1}^{\gamma_2} (a + b \sin^2 \gamma') \sin \gamma' d\gamma'}{\int_{\gamma_1}^{\gamma_2} \sin \gamma' d\gamma'} \qquad (20)$$

where the limits of integration are chosen to include the total angular opening allowed the photo-neutrons and primary gamma rays by the finite size of the detector and toroid. The constants, a and b, represent the number of photo-neutrons projected

into unit solid angle, at the angle $\gamma = 90^{\circ}$, by the magnetic and electric photoeffects, respectively. Table IX presents the values of the integration limits corresponding to each γ-angle; see also Table II above.

TABLE IX

INTEGRATION LIMITS CORRESPONDING TO THE γ-ANGLES

ANGLE, γ		45°	60°	75°	90°
ANGULAR OPENING (γ-rays)		7.8°	8.4°	7.2°	5.1°
ANGULAR OPENING (neutrons)		5°	5°	5°	5°
TOTAL ANGULAR OPENING		12.8°	13.4°	12.2°	10.1°
INTEGRATION LIMIT	γ_1	38.6°	53.3°	68.9°	84.9°
	γ_2	51.4°	66.7°	81.1°	95.1°

Upon integrating equation (20), we obtain for the average intensity at the angle, γ, and for the angular opening from γ_1 to γ_2, the value:

$$\bar{I}(\gamma) = a + b - \frac{b}{3} \frac{(\cos^3 \gamma_1 - \cos^3 \gamma_2)}{\cos \gamma_1 - \cos \gamma_2}$$

The ratio of the intensities corresponding to measurements taken at two different γ-angles will yield information on the value

of the quotient a/b. Designating the ratio of intensities measured at the γ'-angles, γ'_A and γ'_B, by the symbol $B_{A,B}$, we have, therefore:

$$\left(\frac{a}{b}\right)_{A,B} = \frac{B_{A,B}\left\{1-1/3\ \frac{(\cos^3\gamma'_3 - \cos^3\gamma'_4)}{\cos\gamma'_3 - \cos\gamma'_4}\right\} - \left\{1-1/3\frac{\cos^3\gamma'_1 - \cos^3\gamma'_2}{\cos\gamma'_1 - \cos\gamma'_2}\right\}}{1 - B_{A,B}} \qquad (21)$$

where γ'_1 and γ'_2 represent the integration limits associated with the angle γ'_A, while γ'_3 and γ'_4 represent the corresponding limits for the angle γ'_B.

The numerical values for the trigonometric constants in equation (21) appropriate to the four γ'-angle positions of 45°, 60°, 75°, and 90° are presented in Table X. The constant in the last row of this table will, in the discussion to follow, be designated by the symbol $C_{1,2}$ where the subscripts relate to the angles, γ'_1 and γ'_2, representing the limits of integration.

By using the numerical values given in Table X, the experimental ratios of a to b for the several γ'-angle combinations are found from equations (22).

To prepare the experimental data presented in Table VII for use in these equations, it is necessary to apply the corrections discussed in the previous chapter. For this purpose Table XI has been prepared. Here the angular distribution data of Table VII, obtained from each of the six separate tests, are

TABLE X

NUMERICAL VALUES FOR THE TRIGONOMETRIC CONSTANTS

γ-ANGLE	45°	60°	75°	90°
γ_1	38.6°	53.3°	68.9°	84.9°
γ_2	51.4°	66.7°	81.1°	95.1°
$\cos \gamma_1$	.78152	.59763	.36000	.08889
$\cos \gamma_2$	.62388	.39555	.15471	-.08889
$\cos^3 \gamma_1$	.47733	.21345	.04666	.00070
$\cos^3 \gamma_2$	.24283	.06189	.00370	-.00070
$\cos \gamma_1 - \cos \gamma_2$	.15764	.20208	.20529	.17778
$1/3(\cos^3\gamma_1 - \cos^3\gamma_2)$	.07817	.05052	.01432	.00047
$\frac{1/3(\cos^3\gamma_1 - \cos^3\gamma_2)}{\cos \gamma_1 - \cos \gamma_2}$	.49588	.25000	.06975	.00263
$1-1/3 \frac{(\cos^3\gamma_1 - \cos^3\gamma_2)}{\cos \gamma_1 - \cos \gamma_2}$	.50412	.75000	.93025	.99737

recombined according to each γ-angle. The number of counts per minute exclusive of background is evaluated and entered in column 5 of the table. To each of these counting rates, the appropriate decay correction factor and solid angle (Ω) correction factor (columns 6 and 7) are applied to give a corrected counting rate per minute in the last column. The average corrected counting rate per minute at a single γ-angle, designated as $\bar{I}(\gamma)$, for the six sets of data in column 8 is shown at the lower right hand corner of each subdivision of the table.

$$\left(\frac{a}{b}\right)_{45,90} = \frac{.99737\ B_{45,90} - .50412}{1 - B_{45,90}}$$

$$\left(\frac{a}{b}\right)_{60,90} = \frac{.99737\ B_{60,90} - .75000}{1 - B_{60,90}}$$

$$\left(\frac{a}{b}\right)_{75,90} = \frac{.99737\ B_{75,90} - .93025}{1 - B_{75,90}} \qquad (22)$$

$$\left(\frac{a}{b}\right)_{45,75} = \frac{.93025\ B_{45,75} - .50412}{1 - B_{45,75}}$$

$$\left(\frac{a}{b}\right)_{60,75} = \frac{.93025\ B_{60,75} - .75000}{1 - B_{60,75}}$$

$$\left(\frac{a}{b}\right)_{45,60} = \frac{.75000\ B_{45,60} - .50412}{1 - B_{45,60}}$$

TABLE XI

COMPOSITE ANGULAR DISTRIBUTION DATA

1	2	3	4	5	6	7	8
γ-ANGLE	TEST	NO.COUNTS/hr (with backgrd)	AVERAGE BACKGRD/hr	NO.COUNTS/min (less backgrd)	DECAY FACTOR	Ω FACTOR	NO.COUNTS/min (corrected)
45°	1	476	112	6.067	1.0235	2.2293	13.842
	2	392	104	4.800	1.0235	2.2293	10.952
	3	221	90	2.183	1.1965	2.2293	5.824
	4	276	106	2.833	1.1905	2.2293	7.520
	5	381	110.5	4.508	1.0235	2.2293	10.287
	6	308	117	3.183	1.0755	2.2293	7.632
	TOTAL:	2054	639.5				$\bar{I}(45^{\circ})$: 9.343
60°	1	841	112	12.150	1.0780	1.4244	18.656
	2	686	104	9.700	1.0760	1.4244	14.867
	3	386	90	4.967	1.1350	1.4244	8.030
	4	484	106	6.300	1.1320	1.4244	10.158
	5	630	110.5	8.658	1.1315	1.4244	13.955
	6	541	117	7.067	1.0235	1.4244	10.302
	TOTAL:	3568	639.5				$\bar{I}(60^{\circ})$:12.661

TABLE XI (cont'd)

COMPOSITE ANGULAR DISTRIBUTION DATA

1	2	3	4	5	6	7	8
γ-ANGLE	TEST	NO.COUNTS/hr (with backgrd)	AVERAGE BACKGRD/hr	NO.COUNTS/min (less backgrd)	DECAY FACTOR	Ω FACTOR	NO.COUNTS/min (corrected)
75°	1	1171	112	17.650	1.1350	1.1046	22.128
	2	943	104	13.983	1.1360	1.1046	17.547
	3	566	90	7.933	1.0755	1.1046	9.425
	4	721	106	10.250	1.0750	1.1046	12.171
	5	867	110.5	12.608	1.1910	1.1046	16.587
	6	678	117	9.350	1.1920	1.1046	12.311
	TOTAL:	4946	639.5				$\bar{I}(75^{\circ})$:15.029
90°	1	1292	112	19.667	1.1925	1.0000	23.453
	2	1042	104	15.633	1.1925	1.0000	18.643
	3	676	90	9.767	1.0235	1.0000	9.996
	4	860	106	12.567	1.0235	1.0000	12.862
	5	1095	110.5	16.408	1.0765	1.0000	17.664
	6	807	117	11.500	1.1320	1.0000	13.018
	TOTAL:	5772	639.5				$\bar{I}(90^{\circ})$:15.939

The total number of counts per hour and total average background per hour shown at the bottom of columns 3 and 4 of Table XI are used for the calculation of the probable errors in the counting rates. In Table XII these quantities are designated as N_1 and N_2, respectively. The difference between N_1 and N_2 gives the true counting rate, N_o, per hour.

TABLE XII

PROBABLE ERROR OF COUNTING RATE

1	2	3	4
γ-ANGLE	STANDARD DEVIATION $D = (N_1 \neq N_2)^{\frac{1}{2}}$	PROBABLE ERROR .6745D	% PROBABLE ERROR PE/N_o
45^o	$\pm$ 51.89	$\pm$ 35.00	2.47%
60^o	$\pm$ 64.86	$\pm$ 43.75	1.49%
75^o	$\pm$ 74.73	$\pm$ 50.41	1.17%
90^o	$\pm$ 80.07	$\pm$ 54.01	1.05%

Upon applying the average counting rates per minute, $\bar{I}$, of Table XI to the above set of equations (22), we obtain the results given in Table XIII. Column 6 lists the experimentally determined values of $\left(\frac{\overline{a}}{b}\right)$ corresponding to the possible combinations of pairs of γ-angles shown in the first column.

To evaluate the probable error to be assigned each of the quotients, $\left(\frac{\overline{a}}{b}\right)$, it is necessary to propagate the percentage error of Table XII, column 4, through the operations of multi-

TABLE XIII

EXPERIMENTAL VALUES, a/b

1	2	3	4	5	6	7*
POSITIONS COMPARED γ_A , γ_B	$B = \frac{I(\gamma_A)}{I(\gamma_B)}$	$C_{3,4}B$	$C_{3,4}B - C_{1,2}$	$1 - B$	$\left(\frac{\overline{a}}{b}\right)_{A,B} = \frac{C_{3,4} \quad B-C_{1,2}}{1-B}$	PE of $\left(\frac{\overline{a}}{b}\right)$
45° , 90°	.58615	.58461	.08049	.41385	.1945	$\pm$ 0.039
60° , 90°	.79435	.79226	.04226	.20565	.2055	$\pm$ 0.072
75° , 90°	.94288	.94040	.01015	.05712	.1777	$\pm$ 0.263
45° , 75°	.62166	.57830	.07418	.37834	.1961	$\pm$ 0.043
60° , 75°	.84247	.78371	.03371	.15753	.2140	$\pm$ 0.097
45° , 60°	.73789	.55342	.04930	.26211	.1881	$\pm$ 0.063

* Extracted from Column 8, Table XIV

plication, subtraction, and division as required by equations (22). For this purpose Table XIV has been prepared in which the numerical values resulting from the stepwise processes of the computations are listed successively in the columns of this table. In column 7, the resulting percentage probable error of $\left(\frac{\overline{a}}{b}\right)$ is shown for each combination of pairs of angles. It will be noted that the error for the 75°, 90° combination is over 147%. This large error results quite naturally from the fact that the ratio of neutron intensities, B, for these two positions differs only slightly from unity, i.e., .94288, as seen in column 2, Table XIII. Consequently the difference $(CB_{75,90} - C)$, column 4, Table XIII, is small and the percentage probable error associated with this difference (column 5, Table XIV) is large. It may be readily shown that, to reduce the error of $\left(\frac{\overline{a}}{b}\right)$ for the 75°, 90° positions to 50%, would require that $B_{75,90}$ be measured to an accuracy of approximately five-tenths of one percent. This would necessitate that the total number of neutrons detected at each of the two positions be of the order of 50,000. Because of this intrinsic weakness in the analytical treatment of the data, the value $\left(\frac{\overline{a}}{b}\right)_{75,90}$ in column 6, Table XIII, is disregarded in evaluating the weighted average for $\left(\frac{\overline{a}}{b}\right)_{A,B}$.

Because the percentage probable error of the counting rate (column 4, Table XII) is larger the smaller the γ-angle, the percentage error of $\left(\frac{\overline{a}}{b}\right)$, which involves intensity measurements

TABLE XIV

PROPAGATION OF PROBABLE ERROR

1	2	3	4	5	6	7	8
POSIT. COMPRD.	% PE of B	PE of B	PE of $C_{3,4}{}^{B}$	% PE of $C_{3,4}{}^{B} - C_{1,2}$	% PE of 1 - B	% PE of $\left(\frac{a}{b}\right)$	PE of $\left(\frac{a}{b}\right)$
γ_A, γ_B	$\sqrt{\sum(\%)^2}$	(%PE of B)·(B)	(%PE of B)·(CB)	$\frac{\text{PE of } C_{3,4}{}^{B}}{C_{3,4}{}^{B} - C_{1,2}}$	$\frac{\text{PE of B}}{1 - B}$	$\sqrt{\sum(\%)^2}$	(%PE of $\frac{a}{b}$)·($\frac{a}{b}$)
45°,90°	2.68%	± 0.0157	± 0.0157	19.47%	3.80%	19.83%	± 0.0386
60°,90°	1.82%	± 0.0145	± 0.0144	34.12%	7.03%	34.83%	± 0.0716
75°,90°	1.57%	± 0.0148	± 0.0148	145.46%	25.91%	147.74%	± 0.2625
45°,75°	2.73%	± 0.0170	± 0.0158	21.28%	4.49%	21.75%	± 0.0426
60°,75°	1.89%	± 0.0159	± 0.0148	43.94%	10.11%	45.08%	± 0.0965
45°,60°	2.88%	± 0.0213	± 0.0159	32.33%	8.11%	33.33%	± 0.0627

at two γ-angles, varies over wide limits as seen in Table XIV, column 7. For this reason, it is desirable to evaluate a weighted average of $\left(\frac{\overline{a}}{b}\right)$ in such a fashion that greater emphasis is placed on those quotients having the smaller error. To this end, a weighting factor is assigned to each quotient which is inversely proportional to the square of the probable error of that quotient, (column 8, Table XIV). Hence the weighted average of the intensity quotient, $\left(\frac{\overline{\overline{a}}}{b}\right)$, is found from relation (18) of the previous chapter. Applying this averaging process to column 6, Table XIII, we find for a weighted average, the value:

$$\left(\frac{\overline{\overline{a}}}{b}\right) = 0.196$$

The probable error to be assigned to this grand mean is found by application of equation (19), Chapter V, to column 8 of Table XIV. This gives, altogether:

$$\left(\frac{\overline{\overline{a}}}{b}\right) = 0.196 \pm 0.024 \qquad (23)$$

Here again, the probable error associated with the 75°, 90° positions has been omitted in the averaging process.

The above experimental result will permit evaluation of the ratio of probabilities of the magnetic to electric effect. This ratio has been designated by the letter τ in equation (14), Chapter II. By equation (15) we see that the relationship between τ and the quotient, $\frac{a}{b}$, is

$$\frac{a}{b} = \frac{2}{3}\tau \tag{24}$$

Thus, for the Na^{24} gamma ray energy of 2.76 Mev, the relative contribution of the photomagnetic to the photoelectric effect is found experimentally to be

$$\tau = 0.295 \pm 0.036 \tag{25}$$

This leads to the following value for the ratio of the photomagnetic cross section to the total photo cross section:

$$\frac{\tau}{\tau + 1} = 0.228 \pm 0.028 \tag{26}$$

We may compare this experimental result with the theoretically predicted values of τ for the same photon energy by evaluating equation (14), namely

$$\tau = \frac{(\mu_p - \mu_n)^2}{4(1 + \alpha a)} \frac{(E + W_1)^2}{(E + W_o)} \frac{(W_1^{\frac{1}{2}} \pm W_o^{\frac{1}{2}})^2}{E\,Mc^2} \tag{14}$$

The physical constants employed are those shown in Table XV. The value of $E + W_1$ is that reported by K. Siegbahn[62]. We use the experimental evidence outlined in Chapter II that the singlet state of the deuteron is virtual; hence, the positive sign in the last factor of equation (14) applies. Further, the magnitude of the range of the nuclear forces, a, which enters through the wave function normalization factor $(1 + \alpha a)$, is a question which remains open. For zero range, the factor has a value of unity;

TABLE XV

TABLE OF PHYSICAL CONSTANTS

PHYSICAL CONSTANT	$h\nu = 2.187$	$h\nu = 2.237$
μ_p	2.7896	2.7896
μ_n	-1.9103	-1.9103
$E \not\leftarrow W_1$	2.758	2.758
E	.571	.521
W_1	2.187	2.237
W_o	.066	.066
Mc^2	931	931
M	1.66×10^{-24}	1.66×10^{-24}
$(1 \not\leftarrow \alpha a)$	1 ; 1.6401	1 ; 1.6474

for the range $a = 2.8 \times 10^{-13}$ cm, the factor has a value of 1.64 where $\alpha = \frac{\sqrt{MW_1}}{\hbar}$. For purposes of comparison, we evaluate τ for both of these ranges. The resulting values are shown in Table XVI.

Within recent months, the work of Bell and Elliott[8] has led to some doubt regarding the heretofore accepted value of $2.187 \not\pm 0.011$ Mev for the deuteron binding energy. These authors give a value of $2.237 \not\pm 0.005$ Mev. The influence of this change upon the value of τ is considerable, amounting to approximately 20%. For this reason Table XVI has been prepared to illustrate also the effect of this change upon the ratio of the magnetic to the electric photoeffects.

TABLE XVI

COMPARISON OF EXPERIMENTAL & THEORETICAL RATIOS,

$$\tau = \frac{\sigma_m}{\sigma_{el}}$$

W_1 (Mev)	τ, EXPERIMENTAL	τ, THEORETICAL	
		Range: Zero	Range: 2.8×10^{-13} cm
2.187	0.295 ± 0.036	0.374	0.228
2.237		0.453	0.275

Finally, a comparison of the above experimental value of a/b with those found by previous investigators will be of interest. In Table XVII these are listed in the chronological order in which they appeared in the literature. The discussion relating to these findings was presented at the end of Chapter III, Section A. All entries in the table are the results of experiments using gamma rays from Na^{24} with the exception of the Graham and Halban value for which the ThC' gamma rays were used.

TABLE XVII

COMPARISON OF EXPERIMENTAL VALUES, a/b

Graham & Halban[25]	Lassen[31]	Hamermesh & Wattenberg[32]	Author
0.26 ± 0.08	0.22 ± 0.04	0.15 ± 0.04	0.196 ± 0.024

The work of Graham and Halban, performed indoors and thereby requiring a 9% correction for wall scattering, was an extremely low intensity experiment requiring several geometrical corrections whose amounts were not easy to estimate.

The work of Lassen, reported as a Letter to the Editor, is only briefly discussed, thereby making a critical evaluation impossible. Here, the author selectively detects the photoprotons by the pulse sizes produced in a battery of proportional counters. By estimation of the location of the peak of a pulse-size distribution curve, the angular distribution of the protons was obtained by determination of the number of protons corresponding to the peak. This procedure is difficult as the peaks are not very well defined. No reference is made of the angular spread allowed the protons for detection. In addition, the large fluctuation in the number of protons detected at the smaller γ-angles, as well as the large error associated with the number of protons recorded at each position, renders the problem of the determination of the intensity at $\gamma = 0^{\circ}$ an extremely difficult one.

The Hamermesh and Wattenberg results, reported briefly in the January 1949 Bulletin of the American Physical Society, Vol. 24, as $a/b = 0.24$, was revised downward after publication of the Bulletin to the value shown in Table XVII. The details regarding this revision have not been published and the corrections are being subjected to further investigation at the present time. This experiment was performed indoors and required

approximately a 20% correction* for the effect of scattering by the walls. In general, the method employed followed closely that used by Graham and Halban, see Chapter III, Section A.

B. Conclusions

We are led by the overall results of this investigation to conclude that, within the accuracy of the experimental error, the observed total angular distribution of the photo-neutrons arising from the photo-disintegration of the deuteron conforms with the theoretical prediction that the distribution is anisotropic with the ejected particles emerging predominantly at right angles to the direction of the incident gamma radiation. The prediction, on theoretical grounds, that this total angular distribution may be resolved into an isotropic component arising from magnetic interaction of the photon with the deuteron and an anisotropic component arising from electric interaction with the deuteron is consistent with the results of this investigation. That the relative magnitude of these two components conforms to the theoretical value as predicted by equation (14) is in general verified. However, neither the accuracy of the present experimental results, nor the ambiguities relating to the values of the physical constants (Table XV) appearing in equation (14) permit unequivocal conclusion that a precise agreement exists between experiment and theory. We may say categorically, however, that within the generality of "order of magnitude" an agreement is found to exist at the gamma ray energy of 2.76 Mev.

*Private communication

In contrast with early photo-disintegration experiments, the existence of a magnetic component is verified beyond any doubt. At the photon energy involved, the total cross section for the magnetic component appears to be approximately 30% of that for the electric component. Further, it has been shown that σ_m constitutes approximately 23% of the total photo-disintegration cross section.

In consequence of the difficulties attending the measurement of the weak effects associated with photo-disintegration by current techniques, verification of the existence of the additional $^3D - {}^3P$ and $^3D - {}^1D$ transitions (see Table I) predicted by non-central force theory, lies well beyond present experimental capabilities. It is highly improbable that a more sensitive technique following the present experimental scheme can be devised to resolve these lower intensity effects. This limitation, plus the difficulties encountered in making more precise measurements on the predominant $^3S - {}^3P$ and $^3S - {}^1S$ transition products, seriously restrict the inferences one may draw on the basis of experimental results. Thus, supporting evidence regarding such fundamental nuclear properties as the character of the nuclear forces or, for that matter, the range of these forces must rely upon information not currently available from experiments on photo-disintegration.

BIBLIOGRAPHY

1. Chadwick, J. & Goldhaber, M. - Nature 134, 237 (1934)
2. Chadwick, J. & Goldhaber, M. - Proc. Roy. Soc. A151, 479 (1935)
3. Stetter, G. & Jentschke, W. - Zeits. f. Phys. 110, 214 (1938)
4. Wiedenbeck, M.L. & Marhoefer - Phys. Rev. 67, 54 (1945)
5. Myers, F.E. & Van Atta, L.C. - Phys. Rev. 61, 19 (1942)
6. Kimura, K. - Kyoto Coll. Sci. Mem. 22, 237 (1940)
7. Stevens, W.E. - Rev. Mod. Phys. 19, 19 (1947)
8. Bell, R.E. & Elliott, L.G. - Phys. Rev. 74, 1552 (1948)
9. Bethe, H.A. & Peierls - Proc. Roy. Soc. A148, 146 (1935)
10. Breit, G. & Condon, E.U. - Phys. Rev. 49, 904 (1936)
11. Massey and Mohr - Proc. Roy. Soc. A148, 206 (1935)
12. Frohlich, Heitler and Kahn - Proc. Roy. Soc. A174, 85 (1940)
13. Rarita, Schwinger and Nye - Phys. Rev. 59, 209 (1941)
14. Bethe, H.A. & Bacher, R.F. - Rev. Mod. Phys. 8, 83 (1936)
15. Fermi - Ricerca Scient. 7, 2 (1936)
16. Wigner, E. - Phys. Rev. 51, 106 (1937)
17. Hanstein, H.B. - Phys. Rev. 59, 489 (1941)
18. Bethe, H.A. - "Elementary Nuclear Theory," John Wiley & Sons (1947)
19. Schultz and Goldhaber - Phys. Rev. 67, 202 (1945)
20. Frisch, Halban and Koch - Nature 170, 895 (1937)
21. Manley, J.H.,Haworth, L.J., & Luebke, E.A. - Phys. Rev. 61, 152 (1942)
22. Rose, M.E. - Nucleonics 3, 57 (1948)

23. Sutton, R.B., Hall,T.,Anderson,E.E.,Bridge,H.S.,DeWire, J.W., Lavatelli, L.S., Long, E.A., Snyder, T., Williams, R.W. - Phy. Rev. 72, 1147 (1947)

24. Shull, C.G., Wollan, E.O., Morton, G.A., & Davidson, W.L. Phys. Rev. 73, 262 (1948)

25. Graham, G.A.R. & Halban, H.v. - Rev. Mod. Phys. 17, 297 (1945)

26. Chadwick, J., Feather & Bretscher - Proc. Roy. Soc. A163, 366 (1937)

27. Richardson, J.R. & Emo, L. - Phys. Rev. 51, 1014 (1937)

28. Richardson, J.R. & Emo, L. - Phys. Rev. 53. 234 (1938)

29. Halban, H.v. - Nature 141, 644 (1938)

30. Amaldi and Fermi - Phys. Rev. 50, 899 (1936)

31. Lassen, N.Q. - Phys. Rev. 74, 1533 (1948)

32. Hamermesh, B. & Wattenberg, A. - Bul. Amer. Phys. Soc. 24, F1 (1949)

33. Jordan, W.H. & Bell, P.R. - R.S.I. 18, 703 (1947)

34. Report No. MonP-323, Monsanto Chemical Co., Clinton Laboratories, "Instructions for Use of A1 Amplifier and Preamplifier"

35. Eccles, W.H. & Jordan, F.W. - Radio Rev. 1, 143 (1919)

36. Hunt, F.V. & Hickman, R.W. - R.S.I. 10, 6 (1939)

37. Cruft Electronics Staff, "Electronic Circuits & Tubes" Pg. 575 (1947)

38. Geiger, H. & Klemperer, O. - Zeits. f. Phys. 49, 753 (1928)

39. Wollan, E.O. & Shull, C.G. - Nucleonics, 3, 8 (1948)

40. Montgomery, C.G. & D.D. - Phys. Rev. 57, 1030 (1940)

41. Stever, H.G. - Phys. Rev. 61, 38 (1942)

42. Korff, S.A. & Present, R.D. - Phys. Rev. 65, 274 (1944)

43. Korff, S.A.- "Electron & Nuclear Counters," Van Nostrand, Pg. 102-108 (1946)

44. Bethe, H.A. - Rev. Mod. Phys. 9, 128 (1937)

45. USAEC, Isotopes Cir. C-4, "Description of Purification & Filling Technique for BF_3 Ionization Chambers," C.P. Baker & J.A. Bistline - July 1947

46. USAEC, Isotopes Cir. C-6, "Laboratory Production of Enriched BF_3 From CaF_2BF_3," R.E.Zedler & R.I. Luman - July 1947

47. Weil, A.S., Reid, A.F. & Dunning, J.R. - R.S.I. 18, 556 (1947)

48. Reid, A.F. - R.S.I. 18, 501 (1947)

49. Zachariasen, W.H. - Proc. Nat. Acad. Sci. 17, 619 (1931)

50. Tazaki - J. Sci. Hiroshima Univ. A10, 55 (1940)

51. Strain, C.V. - Phys. Rev. 54, 1021 (1938)

52. Delsasso, Ridenour, Sherr & White - Phys. Rev. 55, 113 (1938)

53. Barnes & Valley - Phys. Rev. 53, 946 (1938)

54. Livingood & Seaborg - Phys. Rev. 55, 457 (1939)

55. Shoupp, W.E., Jennings, B., & Jones, W. - Phys. Rev. 73, 421 (1948)

56. DuBridge, L.A., Barnes, S.W., Buck, J.H. & Strain, C.V. - Phys. Rev. 53, 447 (1938)

57. Smith, R.V. & Richards, H.T. - Phys. Rev. 74, 1871 (1948)

58. Heyn - Physica 4, 1224 (1937)

59. Baldwin, G.C., & Koch, H.W. - Phys. Rev. 67, 1 (1945)

60. Bateman, H. - Phil. Mag. 20, 704 (1910)

61. Worthing, A.G. & Geffner, J. - "Treatment of Experimental Data," John Wiley & Sons (1943)

62. Siegbahn, K. - Phys. Rev. 70, 127 (1946)

RULES COVERING USE OF MANUSCRIPT THESES
IN THE UNIVERSITY OF MICHIGAN LIBRARY
AND THE GRADUATE SCHOOL OFFICE

Unpublished theses submitted for the doctor's degree and deposited in the University of Michigan Library and in the Office of the Graduate School are open for inspection, but are to be used only with due regard to the rights of the authors. For this reason it is necessary to require that a manuscript thesis be read within the Library or the Office of the Graduate School. If the thesis is borrowed by another library, the same rules should be observed by it. Bibliographical references may be noted, but passages may be copied only with the permission of the authors, and proper credit must be given in subsequent written or published work. Extensive copying or publication of the thesis in whole or in part must have the consent of the author as well as of the Dean of the Graduate School.

This thesis by .....
has been used by the following persons, whose signatures attest their acceptance of the above restrictions.

A Library which borrows this thesis for use by its readers is expected to secure the signature of each user.

NAME AND ADDRESS DATE

Form 6327 8-47 1M